NONLINEAR CHARACTERISTICS OF WAVE PROPAGATION OVER VEGETATION

A Thesis

by

ARAVINDA BHARATHI VENKATTARAMANAN

Submitted to the Office of Graduate and Professional Studies of
Texas A&M University
in partial fulfillment of the requirements for the degree of

MASTER OF SCIENCE

Chair of Committee,	James Kaihatu
Committee Members,	Scott Socolofsky
	Chris Houser
	Jane Smith
Head of Department,	Robin Autenrieth

May 2014

Major Subject: Ocean Engineering

ABSTRACT

The attenuation of wave energy by submerged or near-emergent coastal vegetation is one of the prominent methods of energy dissipation in areas with significant presence of wetlands. In this thesis, the nature of this dissipation in nearshore random wave fields is investigated using a parabolic frequency-domain nonlinear wave model, modified to incorporate different mechanisms which represent energy dissipation by the vegetation. The nonlinear wave model with the various dissipations mechanisms is tested against data, and the performance evaluated.

Two individual dissipation descriptions which give different importance to the effect of vegetation motion on the damping are studied and the model results are compared with available data in literature to determine the importance of plant stem sway. We then further show the effect of vegetation-induced damping on non-linear wave-wave interactions via bi-coherence analysis.

DEDICATION

I would like to dedicate this thesis to my father, Venkattaramanan, who gave me the first equal platform to share and discuss my ideas on any topic, and continues to do so (contrary to popular father-son dynamics in my home country).

ACKNOWLEDGEMENTS

I would like to thank my committee chair, Dr. Kaihatu for his continued support and for all the insights and gentle nudges that have greatly helped me complete the research work and writing of this thesis. I would also like to thank my committee members, Dr. Socolofsky, Dr. Houser, and Dr.Smith, for their guidance and support throughout the course of this research. This work would not have been complete without Dr.Smith's agreement to share the data from experiments in Coastal Hydraulics Laboratory, Vicksburg.

Thanks also goes to my friends, colleagues and the department faculty and staff for making my time at Texas A&M University a great experience.

Finally, thanks to my family for supporting and encouraging me to continue studying and doing what I like, throughout my stay away from them.

NOMENCLATURE

ω	Wave angular frequency
k	Wave number
E	Wave energy per unit wavelength
C_g	Group velocity
ε_D	Rate of wave energy dissipation
ρ	Density of sea water
C_D	Drag coefficient
D	Diameter of plant stem
s	Height of vegetation
h	Total water depth
g	Acceleration due to gravity
b	Horizontal spacing between plant stems
N	Stem density per unit area
A	Local wave amplitude
k_i	Amplitude decay coefficient
F_x	Horizontal drag force
F_z	Vertical drag force
u	Horizontal particle velocity
w	Vertical particle velocity
η	Wave elevation
ϕ	Velocity potential

C	Wave velocity
f	Wave cyclic frequency
H	Local wave height
H_{RMS}	Root-mean-square wave height
R_n	Reynolds number
ν	Kinematic viscosity of water
$S_{\eta\eta}(\omega)$	Spectral amplitude at frequency ω, of power spectrum of wave heights
$\Delta\omega$	Fundamental frequency

TABLE OF CONTENTS

LIST OF FIGURES

LIST OF TABLES

CHAPTER I

INTRODUCTION

1.1 Role of Coastal Vegetation

Coastal vegetation is one of several large scale multi-purpose systems existing in nature. First and foremost, it protects and nourishes countless species of marine and amphibious organisms. As most of the wetlands are found where freshwater interacts with saltwater, they form an important transitional zone, mediating the exchange of nutrients and nutrient-rich sediments (Philips 1989). Wetland plant stems alter the hydrodynamic conditions (Kadlec 1995) thereby indirectly determining the strength and extent of exchanges.

The water flowing through vegetation is found to contain dissolved gases and nutrients that affect the movement of gametes or spores during their reproductive stage (Koehl 1986). These gametes and spores form an essential link in the food chain that leads to cultivation good fisheries (Mottet 1981).

Wetlands also act as a buffer that regulates water levels during the tidal cycles and other flooding events such as hurricane surge (Costanza et al. 2008), as they tend to naturally store water and control its spread uniformly over the area. Other mechanisms that enable vegetation to reduce flood damage during storms include reduction of fetch for generating wind waves, increasing drag on water motion and direct absorption of wave energy.

Flora along the coast influences the movement of sediment alongshore and can aid in formation and expansion of beaches (Liu and Shen 2008). Typically shoreline

protection involves construction of hard structures such as groins and breakwaters. These methods are effective as they hinder and reduce the wave orbital velocities (Price et al. 1968), but they also alter fluctuations of temperature, salinity, water levels and hydrology (Williams and Thom 2001). They also disturb local sediment transport, and nearshore circulation patterns (Macdonald et al. 1994) and are prone to form a system that is in unstable equilibrium. Wetlands can also be used for similar purposes due to their adverse effect on wave energy and tend to quickly assimilate the local wave features and properties and result in stable sustainable beach configuration (Rogers 1987).

1.2 Objective of Study

The primary effect of vegetation on the incident wave field is via dampening of wave energy. This has a profound effect on irregular wave propagation, as this dampening is a function of frequency, affecting the shape of the wave spectrum. As vegetation is also in turn affected by the waves (particularly during storms, in the form of stem breakage), understanding the nature of the feedback between waves and vegetation involves detailed analysis of the dynamics of the wave field.

Further driving this work is the fact that forecasting wave models are being formulated to include shallow water wave characteristics (e.g. Booij et al 1999) to predict near shore wave properties for operational forecasts (Allard et al 2008). This represents a notable break from traditional forecasting domains, which have ranged from global to regional (e.g. Rogers et al. 2007), and is reflective of the need for regular nearshore forecasts (Allard et al. 2008). While these adapted models are well able to

replicate bulk parameters of nearshore waves measurements (peak wave period, significant wave height), their performance is less satisfactory for more detailed statistical measures (skewness, asymmetry, spectral shape). In the nearshore, wave nonlinearity at second order in wave amplitude becomes a larger factor in the process of nearshore wave evolution, and in turn affects free surface and velocity moments, which are identically zero in instances where the irregular wave field is completely linear (Elgar and Guza 1985). These measures are useful for calculating inputs to other process models such as those for instantaneous sediment transport (Bailard 1981). Any comprehensive study of the physical processes in the coastal region, therefore, must allow some degree of non-linearity. This will enable us to determine extent of influence of wave-vegetation interaction on energy exchanges among the frequency bands, the shape of the evolving spectra and statistics of the wave shape.

Various representations of the damping behavior of vegetation will be examined. Historically, much previous work focused on the variation in root-mean-square wave-height (H_{RMS}) as the waves move over vegetation. The general approach has been to develop a mechanism which dictates the manner in which H_{RMS} would change with distance of wave propagation, with parameters based on a drag coefficient representing the drag on the wave motion caused by the individual plant stems (Kobayashi et al. 1993; Mendez and Losada 2004). These bulk representations assumed that the evolution characteristics of the waves were adequately modeled by linear wave theory, and considered neither the nonlinear characteristics of the waves, nor the shape of the resulting spectrum.

In this work, we use a nonlinear, deterministic, phase-resolving shoaling model which tracks evolution of the complex amplitudes of the free surface, coupled with a dissipation formulation for wave-vegetation interaction. One of the main challenges in incorporating these mechanisms into a phase resolving nonlinear wave model is the representation of the drag coefficient for the formulation in question. This is based on Reynolds number, which depends on a characteristic velocity representative of the irregular wave field. Here, we choose the characteristic velocity to be horizontal wave particle velocity at the head of the vegetation stem.

Since we obtain values of spectral amplitudes at various locations along the path of the wave, we will evaluate some higher order properties of waves, such as wave skewness and bicoherence.

1.3 Overview of Thesis

This thesis is organized into four chapters. Chapter I introduces the importance of wetlands, and puts forth the need to have an improved understanding of their interaction with shoaling waves. The first section of this chapter contains an overview of role of wetlands as an important asset to the shorelines. A brief description of the facts that have driven this research, together with its intent is presented in section two.

Three parts comprise Chapter II, which details the advancements in modeling of waves over vegetation. Section one briefly summarizes the need to predict statistics of shoaling waves by using phase-resolved models in the frequency domain. An overview of advantages of using a non-linear model is also included in the same. A few experiments that have propelled studies to determine the underlying nature of wave-

wetland interaction are outlined in section two. Wave attenuation theories for flow through emergent and submerged vegetation are recapitulated in section three.

Chapter III is divided into four parts that present a detailed description of the wave model and the methodology used in this research. A discussion of the non-linear shoaling model is given in section one. Section two reiterates the theory behind the development of various formulations to represent wave attenuation by vegetation and takes note of some of the important parameters like stem density and drag coefficient that influence the simulation. Studies conducted to model flow through vegetation considering them as stiff and flexible cylindrical rods are reviewed in section three. Also, it contains a discussion about various efforts to determine the drag coefficient by either assuming it to be an averaged quantity or using empirical formulations based on other flow parameters (such as Reynolds number or Keulegan-Carpenter number) obtained from experiments. The final section in this chapter presents the methods used in this study to compute drag coefficient using outputs available from the model.

Chapter IV shows a validation of the model and computation of several higher-order wave statistics such as wave shape skewness and bicoherence. The effect of wetlands on spectral shape evolution is illustrated in detail. It also discusses the influence of vegetation motion on its damping characteristics.

Conclusions and avenues to further develop the current work are contained in Chapter V.

CHAPTER II

LITERATURE REVIEW

2.1 Modeling Waves in Shallow Water

One major component of wave transformation in the nearshore is triad nonlinear energy exchange (nonlinear energy exchange between waves of three different frequencies). This energy exchange mechanism comes from quadratic nonlinearity (second order in wave steepness) and arises from near-resonant interaction between wave components.

Resonant interaction occurs when the frequency-vector wavenumber combination of two waves (ω_1, k_1) and (ω_2, k_2) excite waves at ($\omega_1+\omega_2$, k_1+k_2) and ($\omega_2-\omega_1$, k_2-k_1). In deep water, there are no waves which satisfy this condition; one must continue to the third order to see this interaction between quartets of waves (Phillips 1960). In shallow water, waves both approach shore normal in direction and become less dispersive, so the triad resonance condition is generally closer to being satisfied (Phillips 1981a). Additionally, complete satisfaction of the resonant interaction conditions is not necessary, as *near*- resonant interactions are capable of significant energy exchange (Bryant 1973). These interactions force variations in spectral shape over distances of tens of meters (Kaihatu 2003), in contrast to the very slow energy exchange scales at third order in deep water.

Whalin (1971) ascertained the nonlinear transfer of energy from lower to higher frequency components when waves were allowed to shoal over parallel symmetric circular contours. Boczar-Karakiewicz (1972) performed experiments of forced

sinusoidal waves propagating over a flat bottom, in which significant cycling of energy between the fundamental and higher harmonics were evident; this behavior (called *recurrence*) was developed into an analytical solution by Mei and Unluata (1972).

The behavior seen in the above experiments can be replicated in the classical Boussinesq equations, first adapted for waves over varying bathymetry by Peregrine (1976). These equations, first cast in the time domain, were recast into the frequency domain by Freilich and Guza (1984). The resulting equations dictate the evolution of the amplitudes of time-periodic waves, coupled via the nonlinear interaction terms. These models were shown to accurately predict Fourier coefficients of the wave field in field data. Comparison of the power spectrum of sea-surface elevation revealed a significant lower coherence between predictions by linear finite-depth theory and experimental data in regions where nonlinear effects were important (shallower waters). This was corroborated by Elgar and Guza (1985a, 1985b and 1986) whose bispectrum and biphase observations (viz. Kim and Powers 1979) show transfer of energy between sum and difference frequencies. These interactions cause harmonic growth via excitation of modes in frequencies other that peak frequency. They were also noted to be significant contributors to sea-surface elevation skewness and asymmetry.

The advantage of nonlinear models to provide enhanced predictions of wave shape properties was used by Kaihatu (2001), which is an extension of Kaihatu and Kirby (1995), to demonstrate improved comparisons to data from Mase and Kirby (1992) using a fully dispersive nonlinear frequency-domain model.

In addition to wave shape statistics, the use of a nonlinear model has been shown to explain high frequency damping seen in very dissipative environments. For example, Kaihatu et al. (2007) showed that the high frequency energy attenuation seen in muddy areas (Sheremet and Stone 2003) can be explained by nonlinear energy transfer from energetic high frequencies to lower frequencies directly undergoing damping. It is probable that similar characteristics can be seen with vegetation-induced damping.

2.2 Experimental Observations of Waves over Vegetation

The wave-vegetation interaction phenomenon has been investigated via several experiments and field studies. Field experiments often record the variability in wave attenuation as a result of variation in plant species, coverage and wave conditions (Knutson et el. 1982, Moeller et al. 1999, Bradley and Houser 2009).

Knutson et al. (1982) conducted a field study to quantify wave damping in smooth cordgrass marshes in the eastern shore of Chesapeake Bay in Virginia. They reported that more than 50 percent of wave energy was dissipated within the first 2.5 m and a 94% wave height reduction at the end of the considered 30 m length. As wave energy impacting a shoreline is reduced, an increased potential for sediment deposition was observed. It was also concluded from the data that marshes are most effective in damping waves when they are in emergent conditions.

Quantitative evidence for the effectiveness of a salt marsh in attenuating incoming waves over mudflats was presented by Moeller et al. (1999). Comparison of wave spectra obtained from pressure records were found to support the argument that salt marshes can act as an efficient wave energy buffer during several water depth, wind

and wave conditions. It was also found that the wave energy dissipation over salt marshes is four times the corresponding reduction over mudflats. No marked shift of energy from spectral peak to lower frequency was observed, thus displaying no obvious biased dissipation of particular wave frequencies.

Bradley and Houser (2009) analyzed the effect of low-energy oscillatory flow on the seagrass blades' motion and quantitatively studied the influence of blade motion on wave attenuation. Wave attenuation was noted to decrease as the incident wave height was increased. From video evidence, this was observed to be the result of reduced drag due to streamlining of grass blades caused by higher orbital velocities in conditions with higher wave amplitudes. It was also noted that the loss of energy was not uniform over the range of wave frequencies. Waves at the peak frequency were attenuated but waves at lower frequencies were observed to be unaffected by the vegetation.

There have been several attempts to replicate and study waves over wetlands under controlled conditions in laboratory flumes with either natural (Tschirky et al. 2000) or artificial vegetation (Asano et al. 1988, Dubi and Torum 1994, Augustin et al. 2008). These experiments are more often used to conduct parametric studies, where the influence of properties of plant beds is analyzed. By varying one particular property of interest at a time, such as plant stem density, extent of vegetation or incident wave height and period, the flume experiments isolate the effect of that parameter on wave energy dissipation.

Wave energy reduction by four kinds of coastal vegetation (*H. wrightii, S. filiforme, T. testudinum and Z. marina*) commonly found along Gulf Coast, US, was

evaluated by Fonseca and Cahalan (1992) in their laboratory studies. Live plants were collected as intact sods from several sites in Florida. A fairly consistent effect on transmission of wave energy was achieved through the experiments, and it was noted that stem length was one of the most significant parameters that influenced the amount of energy dissipated by the vegetation.

Tshirky et al. (2000) utilized field monitoring and laboratory testing and showed that the plants of bulrush beds reduced wave heights up to 60 percent of the incident wave height. A set of parameters, such as average plant density and plant bed length, that are significant contributors to energy dissipation were identified and an empirical relationship was formulated to determine the energy that was transmitted through bulrushes under typical Great Lakes conditions.

A study by Augustin et al. (2008) compared wave attenuation effects of synthetic emergent and nearly emergent wetland vegetation in varying wave conditions and plant stem densities. The data collected showed that reduction in significant wave height under emergent conditions is 50 to 200 percent greater per wavelength than that of near-emergent conditions for the same plant configuration and wave condition. It was noted that there was little difference between attenuation by flexible and rigid plant stems within the conditions that were tested which largely were corresponding to the turbulent regime ($R_n > 3000$) of flow within the vegetation. The results also suggested weaker dependence of drag coefficient on wave period as the submergence of plant stem was increased.

2.3 Simulation of Wave-Vegetation Interaction

The field observations and laboratory experiments were consistently augmented by efforts to understand, model and replicate the underlying physics of wave-vegetation interaction through various numerical representations. Since coastal wetlands comprise a significant portion of the US bordering the Gulf of Mexico, an area subject to hurricanes and other strong episodic events, they were studied as a possible means of reducing storm wave and flooding intensity via wave diffraction/attenuation.

Camfield (1977) analyzed the generation and propagation of wind-waves in areas covered with submerged and emergent vegetation. A preliminary method to determine wave height transformations through vegetation was developed using high Darcy-Weisbach friction factors to represent flooded wetlands. For a given wind speed and water depth, wave decay over the extent of plant bed was assumed to be equal to the wave decay over a much longer fetch with sand bottom. Existing shallow water wave forecasting curves, together with a decay factor defined by Bretschneider (1952, 1958) were used to compute adjusted fetch length. The method was not verified due to limited data availability.

Darlymple et al. (1984) argued that the effect of vegetation was a localized presence of high energy dissipation in the water column, which causes the waves to attenuate. Wetlands were modeled as arrays of rigid cylinders and wave energy dissipation was calculated to be the work done by depth-averaged drag force, exerted on the cylinders. The National Academy of Sciences (1977) formulation to compute wave

height decay through trees during coastal flooding due to storms, was extended to arbitrary water depth and tree (cylinder) height to be obtained as:

$$\frac{\partial(Ec_g)}{\partial x} = -\varepsilon_D = -2\rho\frac{C_D}{3\pi}\frac{D}{k}\frac{\sinh^3 ks + 3\sinh ks}{3\cosh^3 kh}\left(\frac{gk}{\omega}\right)^3\left(\frac{1}{b^2}\right)A^3 \qquad (2.1)$$

where $E = \frac{1}{2}\rho g A^2$ is the wave energy, c_g is group wave velocity, ε_D is the time-averaged, depth-averaged energy loss due to vegetation, ρ is fluid density, C_D is the drag coefficient (assumed constant), D is the plant/tree stem diameter, g is gravity, k is the wavenumber, ω is the wave frequency, s is the height of tree stem, h is the total water depth, b is the spacing between trees/cylinders and A is the wave amplitude.

This formulation was developed assuming that linear theory of wave propagation was applicable in water column which included submerged vegetation. It was to be used when vegetation encountered monochromatic waves. A wave amplitude decay equation was derived using equation (2.1):

$$\frac{A}{A_0} = \frac{1}{1+\alpha x} \qquad (2.2)$$

in which,

$$\alpha = \frac{2C_D}{3\pi}\left(\frac{D}{b}\right)\left(\frac{A_0}{b}\right)(\sinh^3 ks + 3\sinh ks)\left[\frac{4k}{3\sinh kh(\sinh 2kh + 2kh)}\right] \qquad (2.3)$$

is the decay coefficient obtained from equation (2.1) and A_0 is the incident wave amplitude.

A similar exposition to that of Dalrymple et al. (1984) was developed by Kobayashi et al (1993) to derive a model that simulates data obtained from artificial kelp

experiments conducted by Asano et al. (1988). Kobayashi et al. (1993) assumed the vegetation motion was infinitesimally small in comparison to wave amplitude and argued that the wave height decays exponentially as the wave propagates through the vegetation.

A two-dimensional problem of small-amplitude waves propagating over submerged vegetation was articulated and an analytical solution was obtained for monochromatic waves using the exponential wave height decay assumption which is as follows:

$$H = H_0 e^{-k_i x} \tag{2.4}$$

where, H and H_0 are wave height at any location x and initial wave height respectively. The decay coefficient k_i was derived as an imaginary component of complex wave number:

$$k = k_r + ik_i \tag{2.5}$$

Within the vegetation the linearized horizontal momentum equation per unit volume was expressed as:

$$\rho \frac{\partial u}{\partial t} = -\frac{\partial p}{\partial x} - F_x \tag{2.6}$$

Linearized drag force used in equation (2.6) to represent dissipation due to presence of stiff cylindrical plant stem, in terms of density (ρ), horizontal velocity (u) and a coefficient (D) is as follows:

$$F_x \simeq \rho D u \tag{2.7}$$

The coefficient D, which was expressed in terms of physical properties of vegetation such as stem height, density and drag coefficient C_D, was used as an indicator of damping of wave energy caused by the drag force.

The analytical solution developed was used to compare with the results obtained by Asano et al. (1988). The measured wave heights were fitted to the exponential decay expression using the method of least squares to calibrate the drag coefficient until the calculated values of k_i equaled the measured values of k_i. The observed trends in wave heights were satisfactorily reproduced by the model and it was inferred that the local flow field was being affected by the vegetation even for the case of small damping.

Waves over vegetation cause some motion in the vegetation, depending on its stiffness. This motion was assumed to be small in most of the previous literature, although experimental evidence (Asano et al. 1988, Dubi and Torum 1994, Bradley and Houser 2009) have shown significant large amplitude sinusoidal motions in low energy flow conditions (R_n < 1000). Mendez et al (1999a) suggested that vegetation motion be incorporated into the governing equations in the vegetation region, in the form of a non-dimensional friction coefficient. This was obtained by normalizing the average work done by the total force on the vegetation (drag and inertial components) with respect to the velocity in the vegetation region (Lorentz hypothesis of equivalent work).

The fluid domain was divided into four regions (as shown in Fig. 1) and the boundary value problem was solved using eigen-function expansion technique after applying appropriate boundary conditions in each of them.

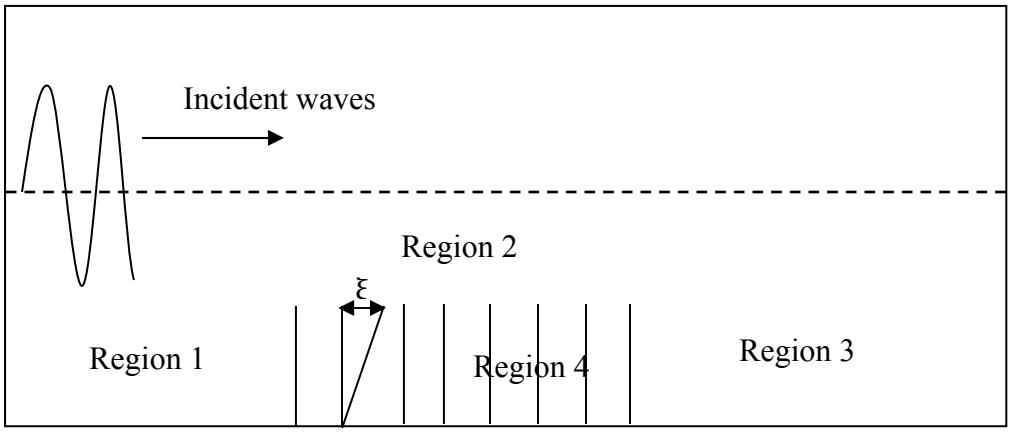

Fig. 1: Sketch of fluid domain (Mendez et al. 1999a)

To facilitate inclusion of stem motion in the vegetation region, drag force was linearized and two factors, λ, an added mass factor and μ, a non-dimensional friction coefficient, were introduced. The added mass factor was derived from stem properties and the friction factor was computed using relative velocity (u_r) and amplitude (ξ) of the vegetation stem motion. The plant stems were assumed to undergo harmonic cantilever type of oscillations and interactions between the stems were ignored.

This model was used to replicate the experimental results of Dubi and Torum (1994). The drag coefficient was used as the calibration parameter and the results from theoretical formulation were in good agreement with the observations.

Presumption of the shape of the wave-height decay curve when comparing model results and data can be seen to be a common practice. Root-mean-square wave height, which is obtained from the area under the wave energy spectrum, cannot be used to compute spectral shape evolution. This is also compounded by the usage of linear theory which results in application of a uniform energy dissipation to all frequencies in the

wave spectrum. But as irregular waves propagate over dissipative medium, change in the shape of the wave spectrum has been observed (Mase and Kirby 1992, Sheremet and Stone 2003) as the waves propagate. This, therefore, deems usage of a non-linear model necessary to obtain evolution of spectrum of irregular waves, which offers a better understanding of energy shifts between frequency bands and to compute other higher order properties.

CHAPTER III

METHODOLOGY

3.1 Nonlinear Model in Frequency Domain

The model used as a basis for nonlinear wave propagation is a one-dimensional version of Kaihatu and Kirby (1995). The model is fully dispersive and uses triad interactions between wave frequencies in intermediate and shallow water; these interactions are *nearly* resonant, which allows for detuned nonlinear interactions caused by dispersive effects. It is generally considered an extension of the model of Freilich and Guza (1984) and Liu et al. (1985).

A wave field, denoted in the terms of free surface elevation $\eta(x,y,t)$, over a spatially varying bottom, $h(x,y)$ is considered by Kaihatu and Kirby (1995). The boundary value problem for the velocity potential, ϕ is formulated as:

$$\nabla_h^2\phi + \phi_{zz} = 0; \qquad -h \le z \le \eta \tag{3.1}$$

$$\phi_z = -\nabla_h h.\nabla_h\phi; \qquad z = -h \tag{3.2}$$

$$g\eta + \phi_t + \frac{1}{2}(\nabla_h\phi)^2 + \frac{1}{2}(\phi_z)^2 = 0; \qquad z = \eta \tag{3.3}$$

$$\eta_t - \phi_z + \nabla_h\eta.\nabla_h\phi = 0; \qquad z = \eta \tag{3.4}$$

where ∇_h denotes the gradient operator in horizontal coordinates (x,y) and g is the acceleration due to gravity.

As the free surface boundary conditions are applied at a position not known *a priori*, they are expanded using Taylor series about $z = 0$. Also, due to nonlinearity of the conditions, terms smaller than $O(\varepsilon^2)$ are ignored and the resulting equations are:

$$\nabla_h^2\phi + \phi_{zz} = 0; \qquad -h \le z \le 0 \tag{3.5}$$

$$\phi_z = -\nabla_h h.\nabla_h\phi; \qquad z = -h \tag{3.6}$$

$$g\eta + \phi_t + \frac{1}{2}(\nabla_h\phi)^2 + \frac{1}{2}(\phi_z)^2 + \eta\phi_{zt} = O(\varepsilon^3) \cong 0; \qquad z = 0 \tag{3.7}$$

$$\eta_t - \phi_z + \nabla_h\eta.\nabla_h\phi - \eta\phi_{zz} = O(\varepsilon^3) \cong 0; \qquad z = 0 \tag{3.8}$$

$\varepsilon = (ka$, where k is the wave number and a is a characteristic wave amplitude) is the nonlinearity parameter.

Assuming a superposition of solutions, similar to approach of Smith and Sprinks (1975), the velocity potential is given by:

$$\phi(x, y, z, t) = \sum_{n=1}^{N} f_n(k_n, h, z)\,\tilde{\phi}_n(k_n, \omega_n, x, y, t) \tag{3.9}$$

As the model seeks to extend its validity to deeper waters, the frequency, ω_n and k_n, the wave number of n^{th} frequency component are related by linear dispersion relationship:

$$\omega_n^2 = gk_n \tanh k_n h \tag{3.10}$$

and the depth dependence function f_n is defined by linear theory:

$$f_n = \frac{\cosh k_n(h+z)}{\cosh k_n h} \tag{3.11}$$

To render the governing equations to frequency domain $\tilde{\phi}_n$ is expressed as:

$$\tilde{\phi}_n(x,y,t) = \frac{\hat{\phi}_n}{2} e^{-i\omega_n t} + \frac{\hat{\phi}_n^*}{2} e^{i\omega_n t} \tag{3.12}$$

$$\hat{\phi}_n = -\frac{ig}{\omega_n} A_n(x,y) e^{i\int k_n(x,y)dx} \tag{3.13}$$

where A_n is the complex amplitude and is assumed to be a slowly varying function in horizontal coordinates (x, y).

Applying Green's identity on the variables f_n and $\tilde{\phi}_n$, and allowing resonant triad interaction among three frequency components (Phillips 1981a), equations (3.5) – (3.8), are simplified into the following by using equations (3.9), (3.11) – (3.13).

$$A_{nx} + \frac{(kCC_g)_{nx}}{2(kCC_g)_n} A_n = -\frac{i}{8(kCC_g)_n} \left(\sum_{l=1}^{n-1} RA_n A_{n-l} e^{i\int (k_l + k_{n-l} - k_n)dx} + 2\sum_{l=1}^{N-n} SA_l^* A_{n+l} e^{i\int (k_{n+l} - k_l - k_n)dx}\right) \tag{3.14}$$

In equation (3.14), C and C_g are phase and group velocities respectively. *R* and *S*, are the interaction coefficients that are obtained by substituting triad resonance condition into the governing equations.

$$R = \frac{g}{\omega_l \omega_{n-l}} [\omega_n^2 k_n k_{n-l} + (k_n + k_{n-l})(k_l \omega_{n-l} + \omega_l k_{n-l})\omega_n] - \frac{\omega_n^2}{g}(\omega_l^2 + \omega_l \omega_{n-l} + \omega_{n-l}^2) \tag{3.15}$$

$$S = \frac{g}{\omega_l \omega_{n+l}} [\omega_n^2 k_n k_{n+l} + (k_{n+l} - k_n)(k_l \omega_{n+l} + \omega_l k_{n+l})\omega_n] - \frac{\omega_n^2}{g}(\omega_l^2 - \omega_l \omega_{n+l} + \omega_{n+l}^2) \tag{3.16}$$

Equation (3.14) is further improved upon by Kaihatu (2001), by incorporating a second-order relationship between ϕ and η in the truncated dynamic free-surface boundary condition (eq. 3.3). The following expression for amplitude was assumed:

$$\eta = \sum_{n=1}^{N} B_n e^{i\left(\left(\int k_n dx\right) - \omega_n t\right)} + conjugate \tag{3.17}$$

which resulted in:

$$B_n = A_n + \frac{1}{4g}\left(\sum_{l=1}^{n-1} I A_n A_{n-l} e^{i\int (k_l + k_{n-l} - k_n)dx} + 2\sum_{l=1}^{N-n} J A_l^* A_{n+l} e^{i\int (k_{n+l} - k_l - k_n)dx} \right) \tag{3.18}$$

where

$$I = \omega_l^2 + \omega_l \omega_{n-l} + \omega_{n-l}^2 - g^2 \frac{k_l k_{n-l}}{\omega_l \omega_{n-l}} \tag{3.19}$$

$$J = \omega_l^2 - \omega_l \omega_{n+l} + \omega_{n+l}^2 - g^2 \frac{k_l k_{n+l}}{\omega_l \omega_{n+l}} \tag{3.20}$$

Equation (3.14) is the primary evolution formulation for complex wave amplitudes, A_n , but the free surface elevation is obtained from equations (3.17)-(3.20).

The wave energy loss due to change in seabed conditions or breaking is included by introducing a damping term $\alpha_n A_n$ in the left hand side of equation (3.14). The form of α_n depends on the frequency dependency of the dissipation that is considered. Kaihatu and Kirby (1995) simulated waves shoaling and breaking over a variable bottom, and for this purpose, the simple model of Thornton and Guza (1983) was used to incorporate the change of energy flux due to wave breaking.

$$\left(E\sqrt{gh}\right)_x = -\frac{3\sqrt{\pi}}{16}\rho g \frac{B^3 \tilde{f}}{\gamma^4 h^3} H_{rms}^5 \tag{3.21}$$

where, E is the wave energy at any location x , $\tilde{f}$ and γ are characteristic frequency of the incident wave spectrum and ratio of H_{rms} to the water depth, h respectively. The dissipation mechanism of Thornton and Guza (1983) is based on a narrow-banded process, and additional assumptions need to be imposed to accommodate its inclusion into a frequency domain phase-resolving model. Kirby and Kaihatu (1996) presented a physical argument for distributing the dissipation across the frequency range as a weighted function of frequency squared; this was confirmed by Kaihatu et al. (2007) via analysis of several sets of laboratory data.

Equation (3.21) was compared with a simplified form of equation (3.14) to formulate the damping coefficient, α_n, and the following equation was used to compare the model performance to experimental observations in Case 2 of Mase and Kirby (1992).

$$A_{nx} + \frac{(kCC_g)_{nx}}{2(kCC_g)_n} A_n + \alpha_n A_n = -\frac{i}{8(kCC_g)_n}\left(\sum_{l=1}^{n-1} RA_n A_{n-l} e^{i\int (k_l + k_{n-l} - k_n)dx} + 2\sum_{l=1}^{N-n} SA_l^* A_{n+l} e^{i\int (k_{n+l} - k_l - k_n)dx}\right) \tag{3.22}$$

Our objective is to use equation (3.22) to model wave propagation over vegetation by using similar techniques to convert wave energy flux dissipation into a damping term.

3.2 Wave Attenuation Theory

Vegetation submergence ratio, stem density and drag coefficient of the plant stem are a few of the important factors that have been used to parameterize the role of vegetation in many of theories put forth (Dalrymple et al. 1984, Asano et al. 1992, Dubi and Torum 1994, Mendez et al. 1999a, Dean and Bender 2006). Their effect on the potential of vegetation to dampen the incident wave energy is also well documented by many experiments and field observations (Knutson et el. 1982, Asano et al. 1988, Augustin et al. 2009, Bradley and Houser 2009).

Dalrymple et al. (1984) examined the effect of plants on wave heights of monochromatic waves assuming the plants to be rigid cylinders. Averaging the change in energy flux due to presence of vertical cylinders, wave height decay was derived to be inversely proportional to the distance propagated (Eqs 2.1-2.3). It should be noted that the vegetation was assumed to be homogenous. Though the assumption of rigid plant stems ascribes different values to the drag coefficient, it was deemed necessary by the authors to make up for the lack of extensive contemporary experimental/theoretical knowledge of plant motion in flooded conditions. Therefore equations (2.1)-(2.3) can be regarded as a preliminary method to estimate wave characteristics in vegetated regions.

Kobayashi et al. (1993) used an exponential decay assumption to evolve root-mean-square wave height through the vegetation field. The following is a brief overview of the derivation. The problem examined is depicted in Fig. 2, in which x and z are horizontal and vertical coordinates respectively. Height of submerged vegetation is denoted by d, and still water depth is h. We denote η_1 as the free surface elevation

oscillating about $z = 0$ and η_2 is the vertical displacement of the interface between regions above and within the vegetation.

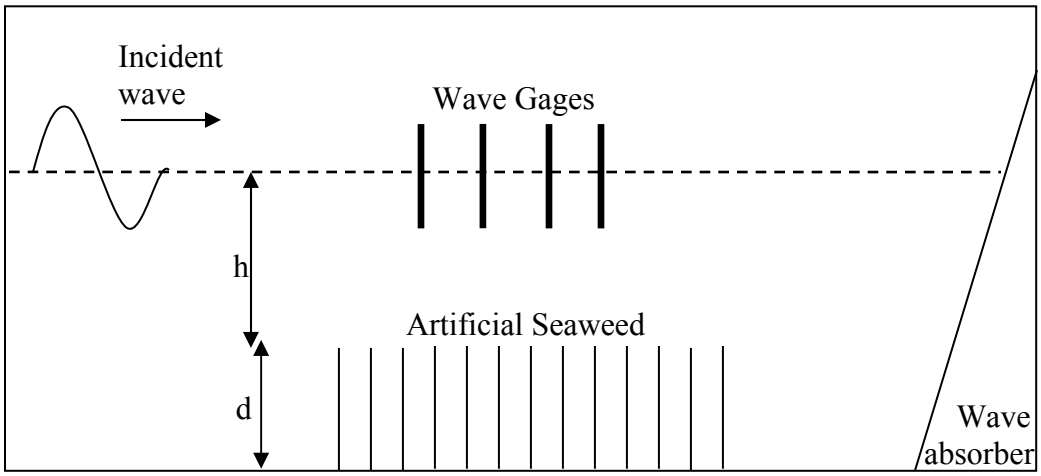

Fig 2: Experimental setup of Asano et al. (1988)

Using standard definitions of horizontal and vertical velocities, u and w respectively, the continuity equations are given by:

$$\frac{\partial u_i}{\partial x} + \frac{\partial w_i}{\partial z} = 0 \tag{3.23}$$

where the subscript $i = 1, 2$ denotes the region above and within the vegetation respectively. The linearized horizontal and vertical momentum equations in region 2 are:

$$\rho \frac{\partial u}{\partial t} = -\frac{\partial p}{\partial x} - F_x \tag{3.24}$$

$$\rho \frac{\partial w}{\partial t} = -\frac{\partial p}{\partial z} - F_z \tag{3.25}$$

in which, F_x and F_z are the horizontal and vertical forces exerted on vegetation by the fluid column per unit volume respectively.

The kinematic and dynamic free surface boundary conditions are linearized akin to development of linear wave theory. At the interface, the kinematic boundary condition is obtained assuming no discontinuity in the interface, i.e., no separation of flow due to vegetation motion. This stems from the assumption that the plant stems exhibit similar behavior to that of rigid vertical cylinders with small diameter, for which drag force is much greater in magnitude than inertial force exerted due to propagation of small-amplitude waves. Horizontal drag force, F_x is obtained using the drag component of Morison's equation (e.g. Dean and Dalrymple 1984) as:

$$F_x \simeq \frac{1}{2}\rho C_D b N |u_2| u_2 \tag{3.26}$$

and the lift force F_z is assumed to be negligible.

$$F_z \simeq 0 \tag{3.27}$$

where C_D is the drag coefficient of plant stem and b and N are plant cross-sectional area per unit stem length and stem density per unit area, respectively. As the motion of the plant stem is not included in the analysis, the velocity used in equation (3.26) is simply the horizontal fluid velocity and not the velocity relative to the plant stem.

The momentum equations are linearized by neglecting the shear stress terms. Therefore the presence of drag force in the region with vegetation results in discontinuity in horizontal velocity at the interface. i.e.,

$$u_1 \neq u_2 \text{ at } z = -h \tag{3.28}$$

Hence, the matching conditions at the interface are given by only:

$$w_1 = w_2 \text{ at } z = -h \tag{3.29}$$

$$p_1 = p_2 \text{ at } z = -h \tag{3.30}$$

Equations (3.23)-(3.25), are solved analytically using equation (2.7), a linearized form of equation (3.26), and assuming the following expression for the free surface elevation:

$$\eta_1 = \frac{H_0}{2} e^{-k_i x} \cos(k_r x - \omega t) \tag{3.31}$$

The incident wave height at $x = 0$ is H_0, ω is the radian frequency of the wave, k_i and k_r are exponential decay coefficient and wave number respectively. In order to reduce the computational effort, a complex wave number, k is defined such that:

$$k = k_r + ik_i \tag{3.32}$$

The time-averaged energy equation for the flow in the entire water column is obtained by adding the individual components, F_1 and F_2 which are the time-averaged energy flux per unit width in regions above and within the vegetation, respectively.

$$\frac{d}{dx}(F_1 + F_2) = -D_d \tag{3.33}$$

Multiplying the momentum equations (eqs. 3.24 and 3.25) with corresponding velocity components (u_2 and w_2) and integrating their time-averages over the depth, after adding the two equations together, yields F_2. The equations for region 1 are used to obtain F_1 in a similar method.

The dissipation D_d is defined as the time-averaged rate of energy dissipation per unit horizontal area due to drag force F_x and is evaluated using the following equation:

$$D_d = \int_{-(h+d)}^{-h} \overline{u_2 F_x} dz \simeq \frac{1}{2} \rho C_D b N \int_{-(h+d)}^{-h} \overline{|u_2| u_2^2} dz \tag{3.34}$$

Assuming weak damping, and using a linearized drag force (eq. 2.7), the analytical solutions obtained for free surface elevation, vertical displacement of the interface, and the dynamic pressures in two regions above and within the plant stems are used to compute F_1 and F_2.

The energy fluxes can be represented using wave energy $E = \frac{1}{8} \rho g H^2$ and group celerity $c_g = \frac{\omega}{2k} \left(1 + \frac{2k_r (h+d)}{\sinh(2k_r (h+d))} \right)$. Equation (3.33) can thus be rendered in the form of standard wave energy budget formulation as follows:

$$\frac{\partial (E c_g)}{\partial x} = -D_d = -\frac{2}{3\pi} \rho C_D b N \left(\frac{k_r g H}{2\omega} \right)^3 \frac{\sinh^3 k_r d + 3 \sinh k_r d}{3 k_r \cosh^3 k_r (h+d)} \tag{3.35}$$

Thus, it can be seen that through this approach, effect of the height, width and density of vegetation stems have been appropriately described. Although, this formulation was verified to be a good representation of wave damping due to vegetation by Kobayashi et al. (1993) through comparisons to experimental results obtained by Asano et al. (1988), the drag coefficient is shown to be a very uncertain parameter, as several iterations were performed by varying drag coefficient until the model results were in good agreement to the laboratory data. This could also be due to fact that drag

coefficient formulation is dependent on the wave conditions and physical properties of vegetation. Thus an exact description would need extensive laboratory study of various types of plant stems and wave conditions prevalent in the coastal wetlands.

In addition to numerical models, several experimental studies have also verified the uncertainty in the drag coefficient (Dubi and Torum 1994, Augustin et al 2008, Bradley and Houser 2009). Therefore, analysis of various representations for drag coefficient is to be done before making an effort to model spectral evolution through vegetation.

3.3 Wave-Vegetation Interaction

Frictional effects of vegetation on waves and flow over them have been the focus of several modeling studies. These studies have mainly resulted in development of expressions and parameterizations for 1-dimensional (or 2-dimensional) frictional drag.

The drag coefficient for any element in a flow is determined by its wake structure (Dean and Dalrymple 1984). Hence, it depends of the Reynolds number, $R_n = Ud / \nu$ where ν is the kinematic viscosity, U and d are characteristic velocity of the flow and characteristic dimension of the element in the direction of flow respectively. Through field observations in near-shore conditions, R_n has been found to be O (1-10^3) (Hammer and Kadlec 1986, Leonard and Luther 1995), a range which covers both laminar and turbulent wake structures.

Kiya et al. (1980) investigated the effect of transverse velocity gradient on vortex shedding frequency due to a circular cylinder in a moderate Reynolds number ($35 < R_n < 1500$) flow and noted that the critical R_n, where the vortex shedding was

initiated, was higher in the presence of the cylinder. The characteristics of flow past two cylinders in tandem were analyzed by Bokaian and Geoola (1984) and later by Luo et al. (1996). The former was more interested in the "galloping" motion of the downstream cylinder, but it was noted that the transverse extent of drag force on the downstream cylinder increased as stem gap increased. Through experiments, it was also observed that, for R_n of 2600, a limited increase in R_n does not affect the change in drag coefficient due to change in separation distance. Luo et al. (1996) examined flow over cylinders with very small spacing and observed reduced drag on the downstream cylinder due to lower surface pressure differential, which is a result of turbulence enforced delay in point of separation on the downstream cylinder.

Nepf et al. (1997) adapted a random walk model to describe the contribution of stem wakes to the turbulent diffusivity within marsh grasses. Although it produced excellent agreement with a simple plant-like array of rigid cylinders, to predict diffusivity of canopies that contain complicated morphology with more flexible members, the wake structure of the flow around the individual element has to be characterized as a function of plant characteristics. Vegetative drag was linked to generation of turbulence intensity to model turbulence diffusivity by Nepf (1999). It was postulated that using drag to describe turbulence intensity can improve our understanding of particle dispersal in coastal marsh systems.

The brief literature review conducted above demonstrates the importance of drag force on the cylinder/stem in the description of flow through vegetation. Wave modelers have largely considered horizontal drag force (eg. equations 3.26 and 3.27) and

neglected the lift force, while defining external forces in the boundary value problems to describe wave propagation over vegetation.

In the earlier efforts to model waves through vegetation, an averaged drag coefficient is used to represent the effect of vegetation on wave propagation (Dalrymple et al. 1984). This assumes that the plant stems behave as though they are a bundle and the drag force does not vary significantly within the marsh system (Bokaian and Geoola 1984).

Alternatively, efforts have been made to compute the drag force and in turn, drag coefficient, C_D, more precisely. The inability to capture the details of the feedback mechanism between change in wave parameters and change in plant motion has hampered representation of flow through vegetation accurately.

Solutions to the problem of vegetation motion have been attempted by Asano et al. (1992), Dubi and Torum (1994) and Mendez et al. (1999), by representing plant stem motion as a forced vibration with one degree of freedom. The equation of motion is linearized either by depth-averaging the equation or assuming linear profiles for plant stem amplitude and water particle velocity or both. The resultant equation is used to calibrate the drag coefficient C_D (by using Morrison's equation for drag force), by having prior knowledge of the nature of the velocity field through measurements.

The drag coefficient C_D used in the simulations carried out in this thesis were obtained from Kobayashi et al. (1993) and Mendez et al. (1999a). Both used a calibrated drag coefficient in their respective models, derived by fitting their model results to the corresponding experimental observations.

The following equations describe the relationship between C_D and R_n.

$$C_D = \left(\frac{2200}{R_n} \right)^{2.4} + 0.08 \tag{3.36}$$

$$C_D = \left(\frac{2200}{R_n} \right)^{2.2} + 0.08 \tag{3.37}$$

$$C_D = \left(\frac{4600}{R_n} \right)^{2.9} + 0.4 \tag{3.38}$$

Equation (3.36) is obtained by Kobayashi et al. (1993) with the assumption that the plant stems behave as rigid cylinders. The range of R_n was between 2200 and 18000 in the experiments conducted by Asano et al. (1988), for which the model was developed. It was observed that C_D decreased with increase in R_n. As the plant stem diameter was constant in the experiments, this led to the conclusion that C_D decreased as characteristic velocity u_c increased. The characteristic velocity used to compute R_n is obtained from the wave particle velocity encountered by the vegetation. This was partially explained by the fact that, in monochromatic wave propagation, as velocity increases, the rigid plant stem tends to attain a slightly bent configuration if the phase of velocity is same as that of the negligibly small amplitude of plant motion. This reduces the surface available to impede the flow (Bradley and Houser 2009).

Mendez et al. (1999a) retained the vegetation motion in their model to derive equations (3.37) and (3.38) for model runs without and with stem motion respectively. It is to be noted that $200 < R_n < 15500$ for equation (3.37). Although, they are representation of flow over vegetation assumed to be rigid cylinders, the difference in

eq. (3.36) and eq. (3.37) could be due to the fact that Mendez et al. consider evanescent modes of wave propagation after interaction with vegetation field and wave reflection towards wave-maker due to presence of the same.

Equation (3.38) is derived for $2300 < R_n < 20000$ by Mendez et al. including swaying motion of plant stem. The plant motion causes a decrease in the relative velocity which results in an increase in the drag coefficient C_D and equation (3.38) captures that trend quite adequately.

3.4 Computation of Drag Coefficient in Model

The model that is used in this study computes evolution of amplitude of each frequency in an incident spectrum (eq 3.22). This complex amplitude, which varies as the wave propagates, is used to obtain the characteristic velocity needed to compute Reynolds number, R_n in the following way.

From linear theory, for a progressive wave field given by $\eta = A\cos(kx - \omega t)$ we know the horizontal wave velocity,

$$u = \left(\omega \frac{\cosh k(h + d + z)}{\sinh k(h + d)} \right) \eta \tag{3.39}$$

where h is the water depth above vegetation, d is the height of plant stem and z is the vertical coordinate of any location in the water column. (Fig 2)

If the wave field is irregular, then the power spectral density, $S_{\eta\eta}(\omega)$ and the complex amplitude A_n (used in equation 3.22) of frequency component ω_n, are related as:

$$S_{\eta\eta}(\omega_n) = \frac{1}{2}\left(\frac{A_n^2}{\Delta\omega}\right) \tag{3.40}$$

Using properties of spectral analysis, the power spectral density of velocity u can be obtained as:

$$S_{uu}(\omega_n) = \left(\omega_n \frac{\cosh k(h+d+z)}{\sinh k(h+d)}\right)^2 S_{\eta\eta}(\omega_n) \tag{3.41}$$

$$u(\omega) = \sqrt{2 * \Delta\omega * S_{uu}(\omega)} \tag{3.42}$$

where $\Delta\omega$ is the fundamental frequency.

Assuming the plant stem undergoes forced harmonic oscillation (cantilever type motion) due to presence of waves, the sway motion at the head of the plant will be the maximum. Consequently, the horizontal velocity at the head of plant stem ($z = -h$) will be the most affected due to the plant stem oscillation and will play an important role in damping the flow field energy. Therefore, the velocity at that location is used as the characteristic velocity of the flow to compute the Reynolds number,

$$R_n = \frac{u(\omega) * d}{\nu} \tag{3.43}$$

which can be used together with equations (3.36)-(3.38) to compute drag coefficient C_D.

The wave energy dissipation term derived by Kobayashi et al. (1993) (eq. 3.35) is used along with C_D defined by Kobayashi (1993) and Mendez (1999a) and the results of spectral evolution obtained using equation (3.22) are provided in the following section.

CHAPTER IV

VALIDATION AND RESULTS

4.1 Validation of the Model

4.1.1 Experiments by Dubi and Torum (1994)

The model described in the previous chapter was to be verified and validated with experimental results available in the literature. After reviewing several laboratory studies, the model was used to recreate the evolution of root-mean-square wave height from experimental data obtained by Dubi and Torum (1994).

Dubi and Torum (1994) studied the dissipative characteristic of artificial Norwegian Kelp using propagation of irregular random waves. Kelp (Fig. 3) is a macroalga that grows on hard surfaces, consisting a stem (stipe) which may be as long as two meters in a fully grown kelp.

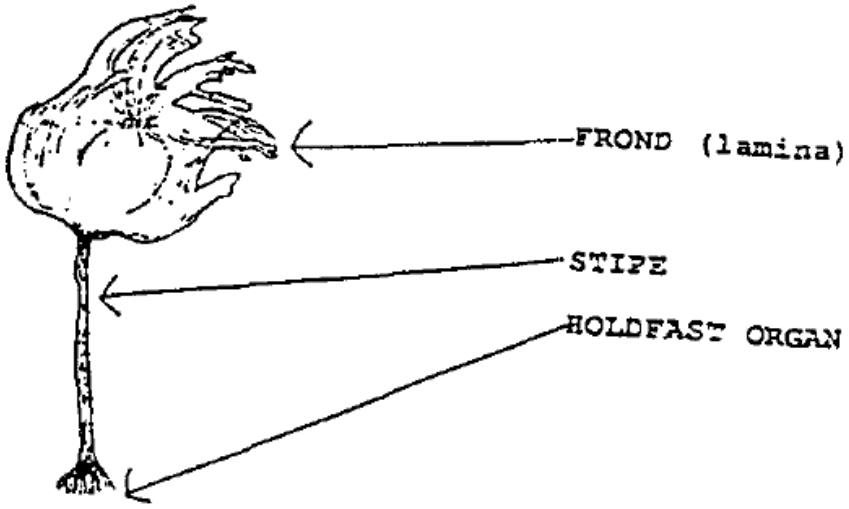

Fig. 3: Description of a Norwegian Kelp (Dubi and Torum 1994)

The experiment was conducted in a 33m long, 1 m wide and 1.6 m high wave tank as shown in Fig 4. The extent of vegetation was set as 9.3 m along the length of wave propagation, approximating a vegetation density of 12 plants per unit square meter. Wave heights were measured using eight wave gauges placed one meter apart from each other starting 17.85 m from wave paddle as shown in Fig 4. In total, 50 tests were carried out with various wave periods.

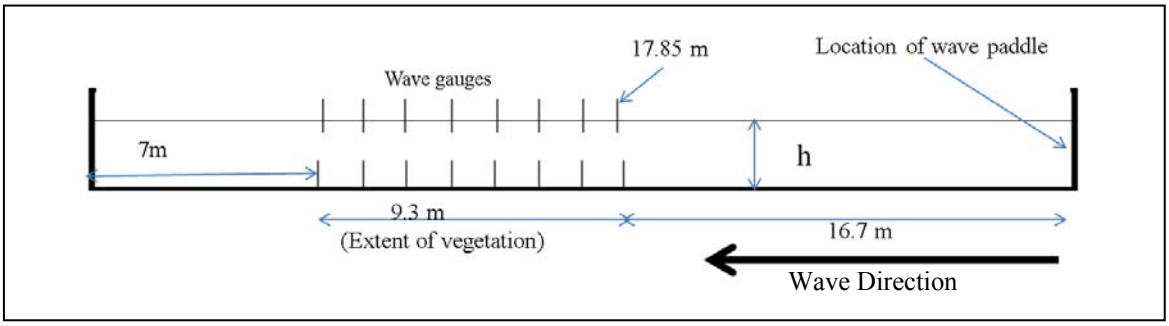

Fig. 4: Experimental Setup of Dubi and Torum (1994).

The Dubi and Torum (1994) data were used by Mendez and Losada (2004) for evaluating their plant dissipation mechanism. Among the results published in Mendez and Losada (2004), we chose to simulate test IR12WD44, which had a peak period of 3.79s and water depth of 0.4m; and IR5WD63, which had a peak period of 1.58s and water depth of 0.6m. The former has a relative depth *kh* of 0.341 that represents intermediate water depth and the latter corresponds to that of deeper water with a *kh* of 1.1727. In both the cases, the vegetation is well submerged in the water column. We do not consider shallower depths because that would lead to emergent stems; in this case the dissipation would need to be represented via a different mechanism.

The wave characteristics of the tests are summarized in the table below:

Table 1: Wave characteristics of selected tests from Dubi and Torum (1994)

	H_{RMS} (m)	T_P (s)	h (m)	h_{veg}/h	kh	R_n (at stem head, approx.)
IR12WD44	0.084	3.79	0.4	0.33	0.341	2014.5
IR5WD63	0.114	1.58	0.6	0.33	1.173	1672.1

4.1.2 Comparison with Model Results

Time series from the experiment were not available, so a synthetic time series was generated for model initialization. The model was run with an input spectrum obtained from time series generated using a TMA spectrum for shallow water with parameter $\gamma = 3.3$ and random phases. This time series was divided into seven realizations of 1024 points each and was converted into Fourier component amplitudes via a Fast Fourier Transform (FFT). These Fourier amplitudes are then used directly for model initialization. Output spectra were obtained at experimental gage locations by Bartlett-averaging the outputs from all seven realizations.

As we have seen earlier, the most important factor in this model is the description of drag coefficient due to presence of the vegetation. This has been treated using three different descriptions in the tests associated with Dubi and Torum (1994) experiments. Along with stiff-vegetation description of Kobayashi et al (1993) and vegetation-sway included Mendez et al (1999a), we also use bulk C_D, as derived by Mendez and Losada (2004) in their effort to empirically model the same lab data. This bulk C_D was derived as a calibration parameter to fit their model results to the lab results.

A linear model, which is uses equation (3.18) with right-hand-side set to zero, is also run with C_D description of Mendez et al (1999a) for the deep water case. This was done to show that the shape of wave spectrum is unchanged when a linear model is used. Figures 5 and 6 show the evolution of H_{RMS}:

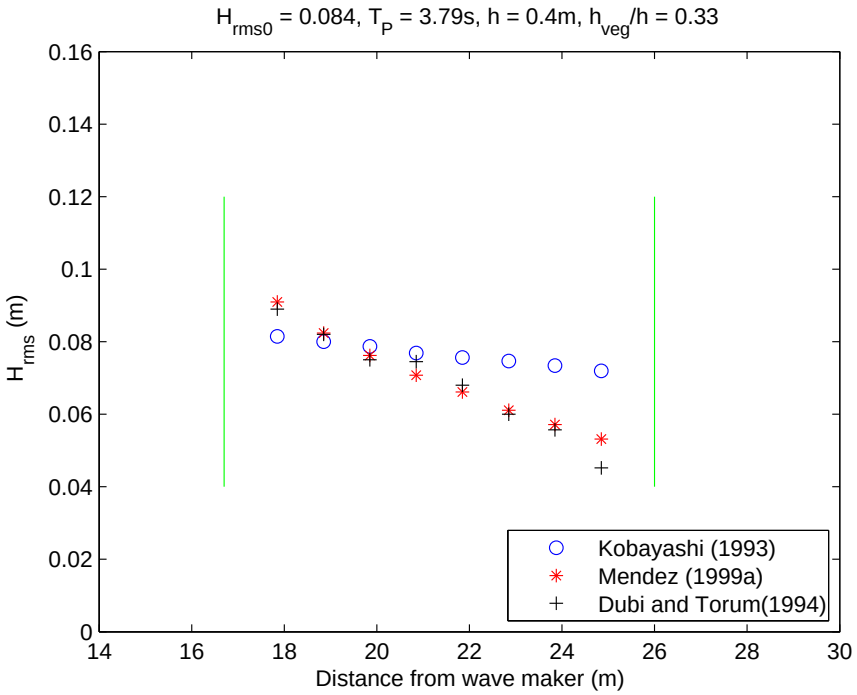

Fig. 5: Evolution of H_{RMS} for Test IR12WD44 from Dubi and Torum (1994)

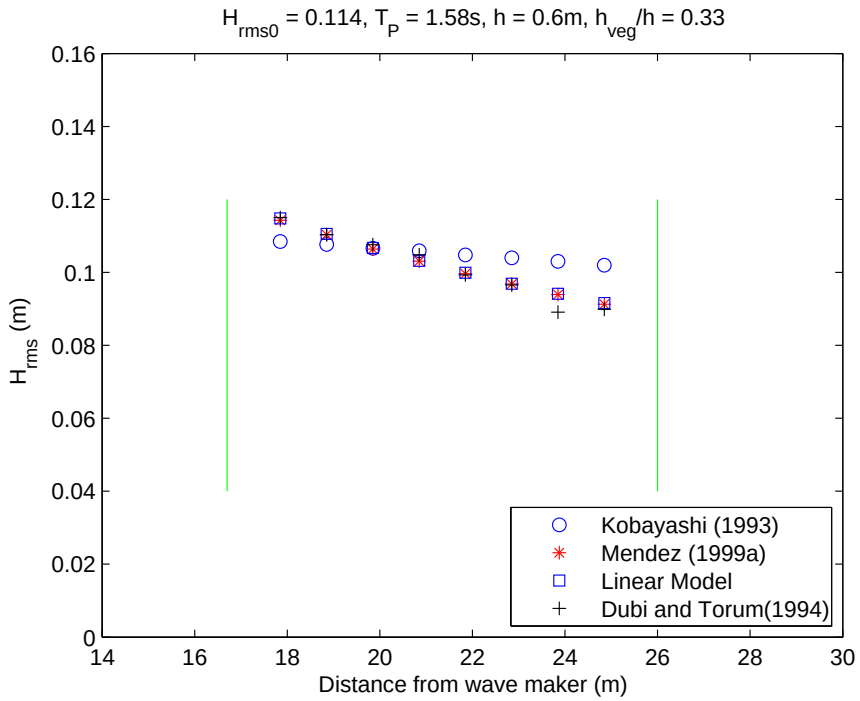

Fig. 6: Evolution of H_{RMS} for Test IR5WD63 from Dubi and Torum (1994)

The green vertical lines in Figures 5 and 6 represent the extent of vegetation; the waves move from left to right in the figure. The performance of the model using Mendez et al (1999a) description for C_D appears to be the most effective. Usage of stiff-vegetation assumption to describe C_D (Kobayashi 1993) seems to underdamp the wave energy, resulting in wide discrepancy in H_{RMS} prediction. This could be explained by the following theory. Using linear theory, the Reynolds numbers of the flow in the experiments have been determined approximately (Table 1) to be of the order of transition and turbulent regime, which is an indication of influence of swaying of vegetation (Mendez et al 1999a). Thus, considering the stem motion has resulted in improved regeneration of the lab results through the model.

Also, we can see that the H_{RMS} evolution predicted by the linear model follows the one predicted by non-linear model (Figure 6), thus verifying the model's ability to predict bulk characteristic such as root-mean-square wave height.

The close match between the linear and nonlinear model estimates of H_{RMS} shows that it is not an adequate metric to evaluate the nonlinear characteristics of the model. The next step is to study the output wave spectra from the nonlinear model and to analyze the evolution characteristics of these spectra. Since no wave spectra were reported in Dubi and Torum (1994), this exercise is less of a model validation than an exploration into the physics of the characteristics of nonlinear spectral evolution over vegetation, but is still instructive.

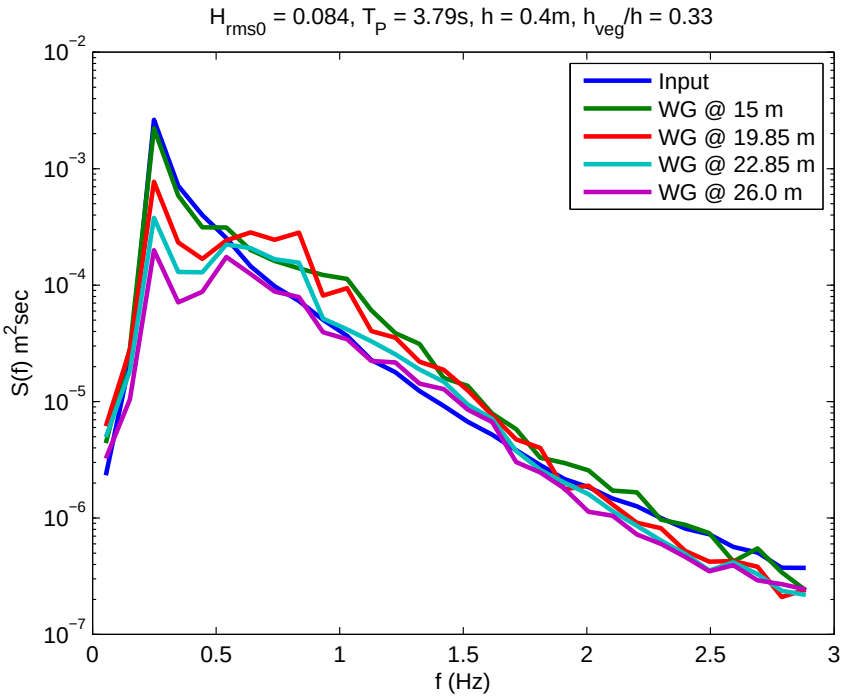

Fig. 7: Evolution of Spectrum for Test IR12WD44 from Dubi and Torum (1994)

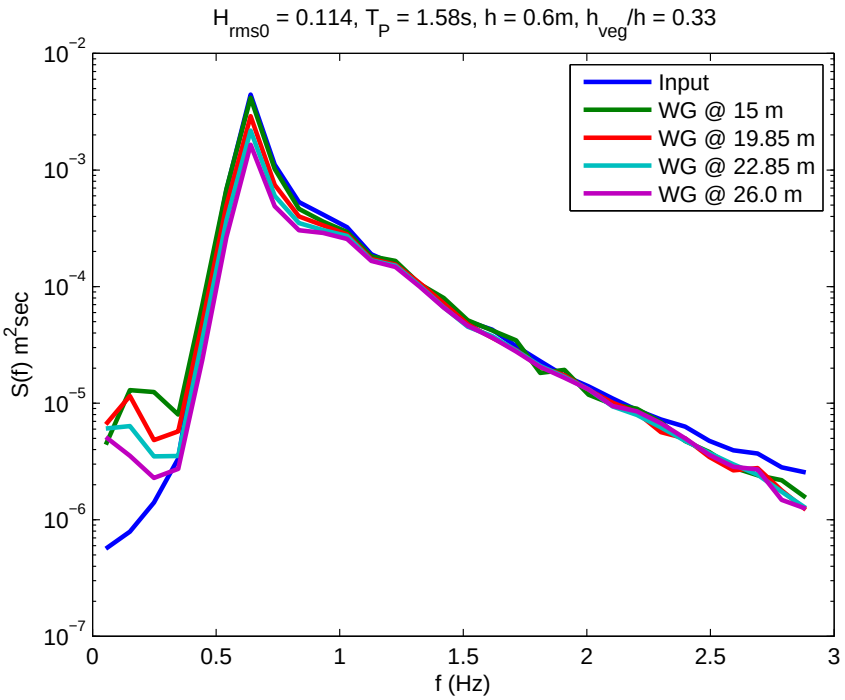

Fig. 8: Evolution of Spectrum for Test IR5WD63 from Dubi and Torum (1994)

The emergence of the second harmonic of the spectral peak in the evolution of spectrum in shallower water depth (Fig 7), indicates distinct flow of energy into regions of twice the peak frequency. This energy transfer to higher harmonics (super-harmonic transfer of energy) is a hallmark of shallow water nonlinear processes. This means exchange of energy between f_p-$2f_p$ could be the strongest in shallower waters. A contrasting case appears in Figure 8; here we can see that there is pronounced sub-harmonic interaction as the frequencies below peak frequency get the most amplified as waves propagate through vegetation. This has implications regarding the use of wetlands as a means of arresting long waves and surge (Williams and Thom 2001), as it appears that in some cases, long wave energy can remain undamped. It can also be observed in

both shallow and deep water cases that the most damped part of the spectrum is that of peak frequency (Anderson and Smith 2013).

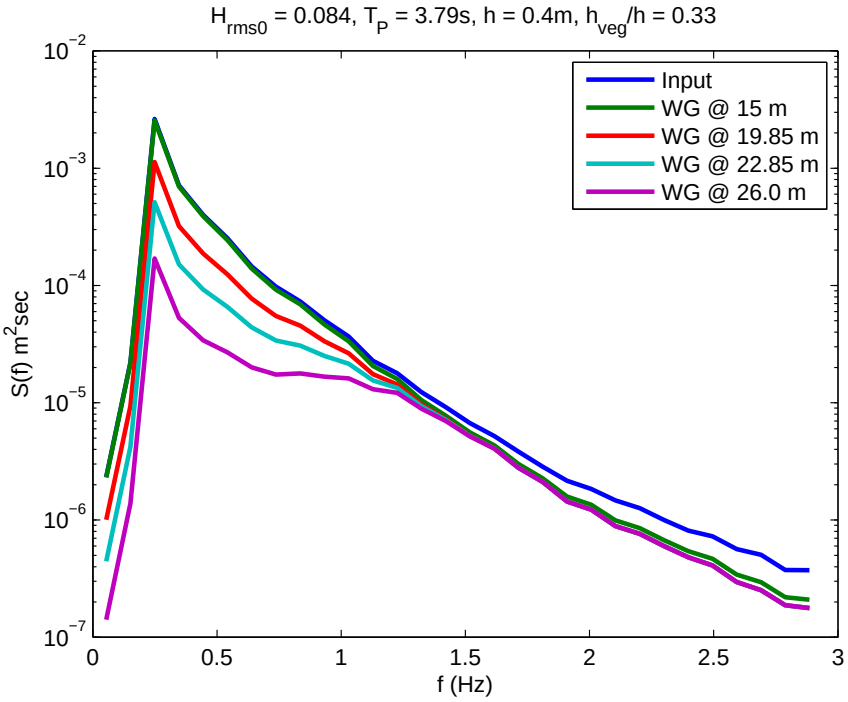

Fig. 9: Evolution of Spectrum for Test IR12WD44 obtained using Linear Model

Spectral evolution of waves in shallow water case (kh = 0.341), obtained using linear model (as described earlier) is shown in Fig 9. Conforming to the nature of models based on linear theory, the spectral shape remains a constant (Elgar and Guza 1985a) in comparison to Fig 7 (which is from non-linear model) as waves move over vegetation.

The spectral energy evolution over the entire course of the experimental setup can be seen in Fig 10, which contrasts the spectral evolution with and without vegetation (the latter being a hypothetical model run). This figure is a false color plot of spectral amplitude densities (red being high) as the random wave train evolves through the

vegetation field (represented by black lines). The damping of energy at peak frequency and evolution of second harmonic can be seen by comparing regions under the black oval.

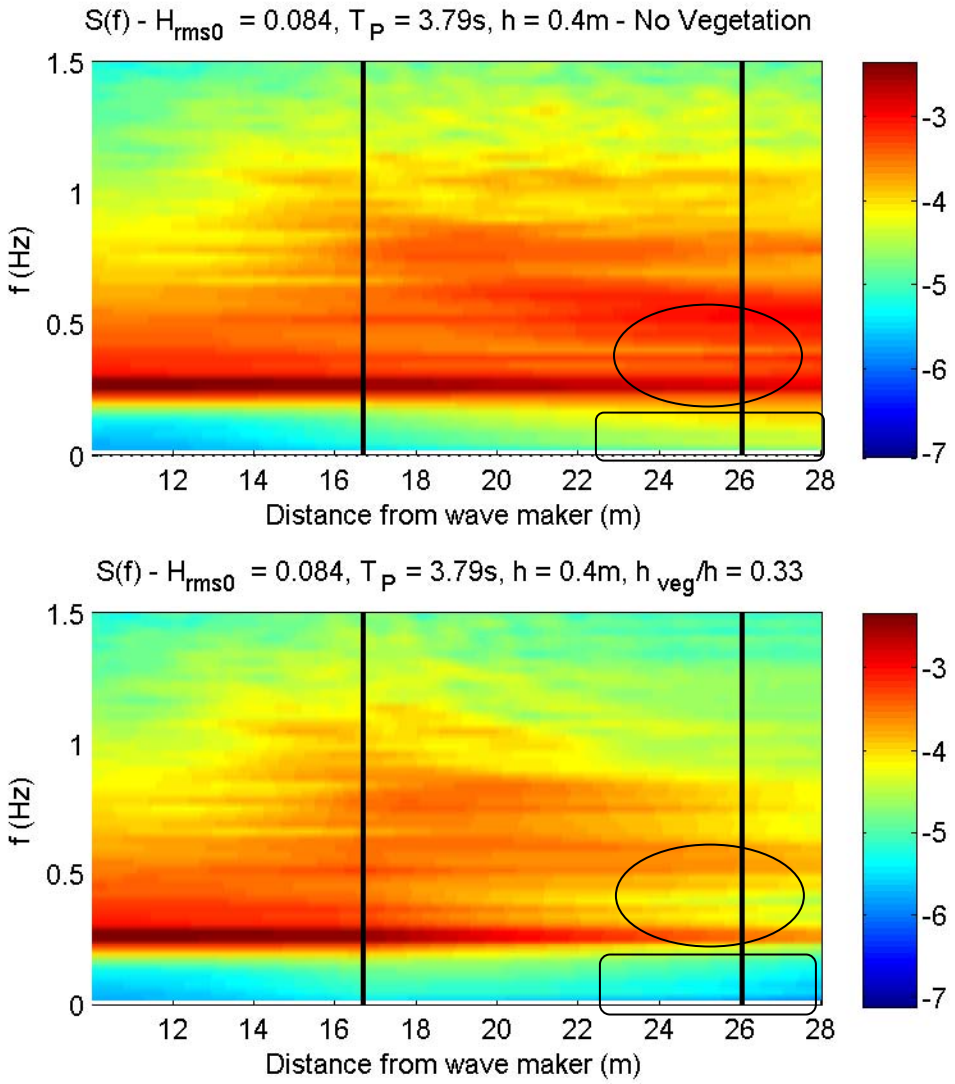

Fig. 10: Evolution of Spectrum for Test IR12WD44 through the test domain

Waves and vegetation submergence conditions similar to ones discussed here can be found when storm surges flood the coastal wetlands. This will lead to additional wave setup (Dean and Bender 2006) and long wave generation resulting in increase in water levels. We can observe that, in shallow water case, evolution of sub-harmonic energy is being suppressed due to the presence of vegetation. This could imply that long wave generation in wetlands during storm surge, will be damped out by the vegetation when the increase in water depth due to flooding is minimal.

4.1.3 Conclusion from study of Dubi and Torum (1994).

As the model has predicted the evolution of H_{RMS} accurately using C_D definition suggested by Mendez et al (1999a), we use the same for simulation of other laboratory experiments, whose analysis is presented in the following section.

4.2 Experiments by Anderson and Smith (2013)

A physical model study to investigate the dissipation of wave energy by artificial *Spartina alterniflora* was conducted in a large-scale two-dimensional flume (Anderson and Smith 2013). *S. alterniflora* is a dominant species of seagrass in the frequently flooded low marsh habitat of Gulf of Mexico and East Coast of United States. (USDA and NRCS, 2012). The study investigates the roles of different factors such as stem density, submergence, incident wave height, and peak period with respect to wave attenuation.

4.2.1 Description of Experiment

The flume measures 63.4m long, 1.5m wide and 1.5m deep. The depth configuration of the flume is as shown in Fig 11. The wave gauge arrangement is

described in Fig 12. The data for 4 different kinds of test scenarios, summarized in the table below, were analyzed and used to initiate the model.

Table 2: Description of test scenarios from Anderson and Smith (2013)

	h, at vegetation (m)	T_P (s)	f_P (Hz)	H_{RMS} (m)	h_{veg}/h
Test 1	0.533	1.5	0.667	0.111	0.78
Test 3	0.533	2.0	0.500	0.111	0.78
Test 6	0.457	1.5	0.667	0.081	0.91
Test 12	0.457	2.0	0.500	0.192	0.91

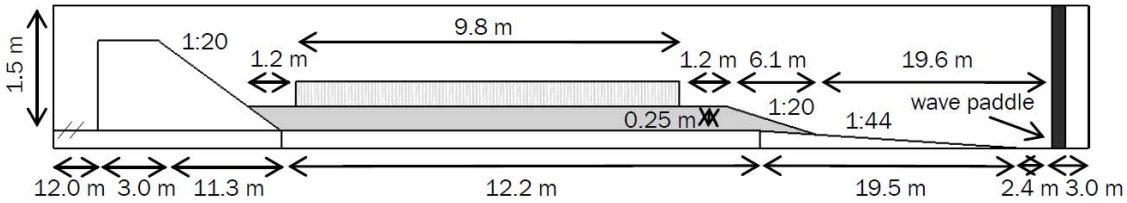

Fig 11: Profile of wave flume (Anderson and Smith 2013)

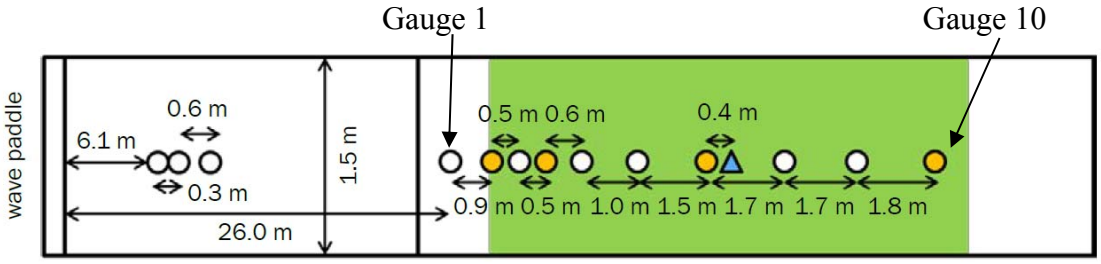

Fig 12: Wave gauge arrangement (Anderson and Smith 2013)

4.2.2 Comparison with Model Results

The model was initiated with the wave spectrum from Gauge 1 (shown in Fig 12), and the data at further gauges were used to compare, validate and interpret the results. The wave elevation time series at Gauge 1 was divided into three realizations of 4096 points each. The model necessitates a maximum value for fundamental frequency, which is dependent of number of points in a realization and sampling rate. Division of time series into more realizations would result in higher fundamental frequency, which causes the model to behave erratically. Complex Fourier amplitudes, obtained by applying FFT on the wave spectrum from each realization was used as input to the model and during post-processing, output spectra were obtained after Bartlett averaging.

Figures 13 and 14 show the evolution of root-mean-square wave height which, as verified earlier with the data of Dubi and Torum (1994), is predicted well by the model. The solid green line represents the extent of vegetation. Tests 6 and 12 too are well simulated through the model and Figure 15 shows the comparison of predicted H_{RMS}, obtained from area under the wave energy spectrum, against the measured value.

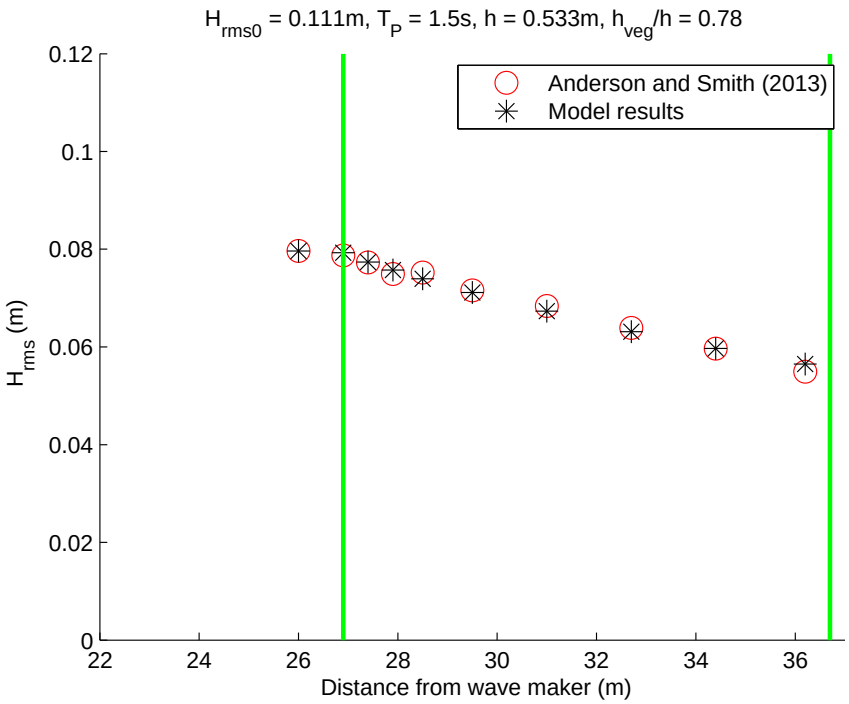

Fig 13: Comparison of wave height evolution for Test 1

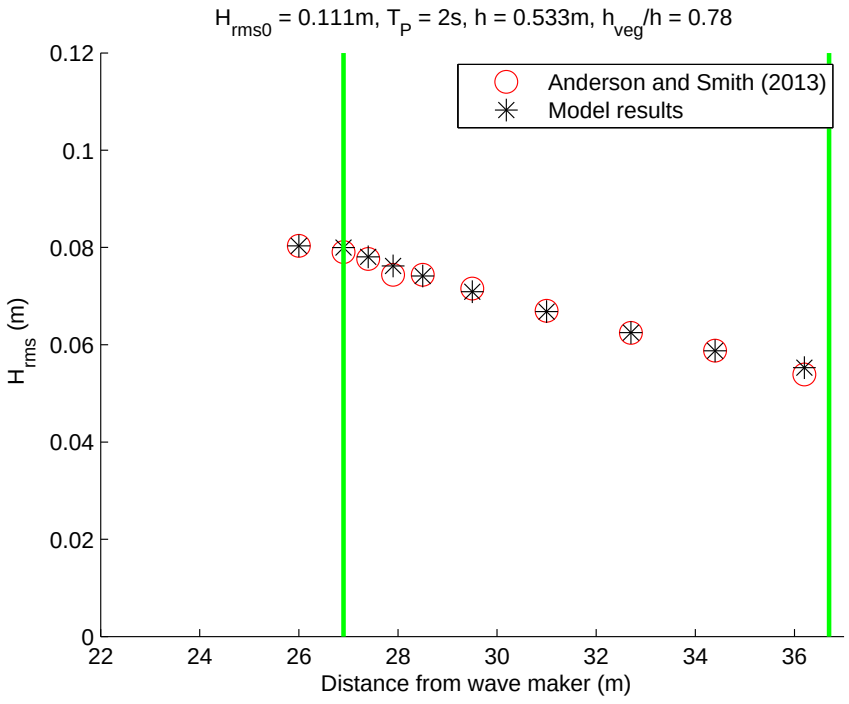

Fig 14: Comparison of wave height evolution for Test 3

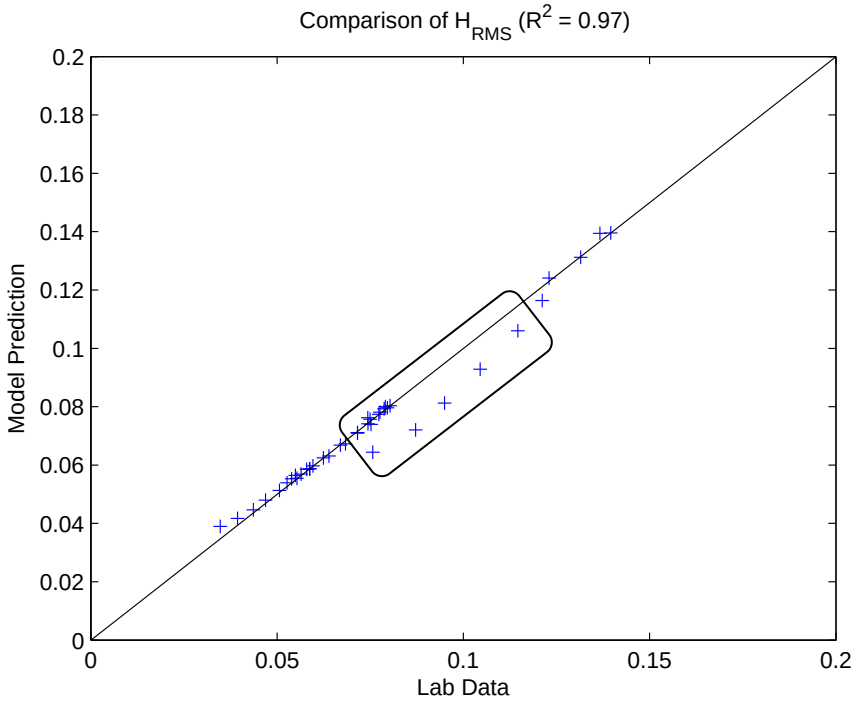

Fig 15: Model Prediction vs Lab Data Comparison for H_{RMS}

Although the H_{RMS} (zeroth order quantity from a spectrum) has been predicted well with the current formulation (Figure 15: $R^2 = 0.97$), it is to be noted that the wave heights in the Test 12 (circled black), which uses an input H_{RMS} that is nearly double of other tests, are off the 45^o line. This could be due to usage of velocity at stem head in the damping formulation. As the wave heights increase, the velocity profile penetrates deeper in the water column, thus exerting more drag force on the vegetation (Nepf 1999). This results in higher damping. Therefore, usage of a different metric such as depth-averaged velocity in the dissipation formulation may lead to improved comparisons.

We now inspect the change in spectral shape as the wave train propagates through the vegetation. Comparisons for the same are provided below in Figures 16 and 17, which correspond to Tests 1 and 3 respectively.

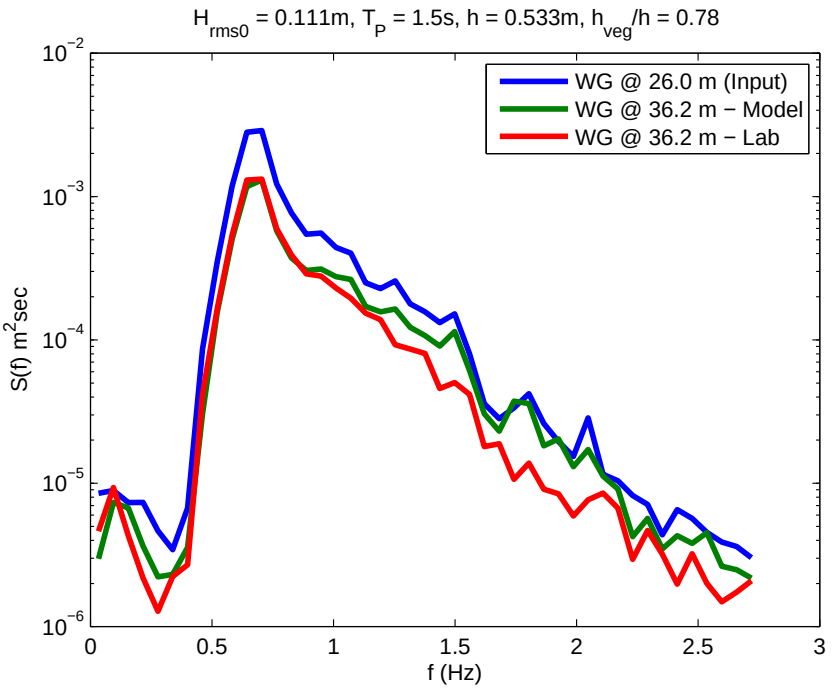

Fig 16: Spectral evolution comparison for Test 1

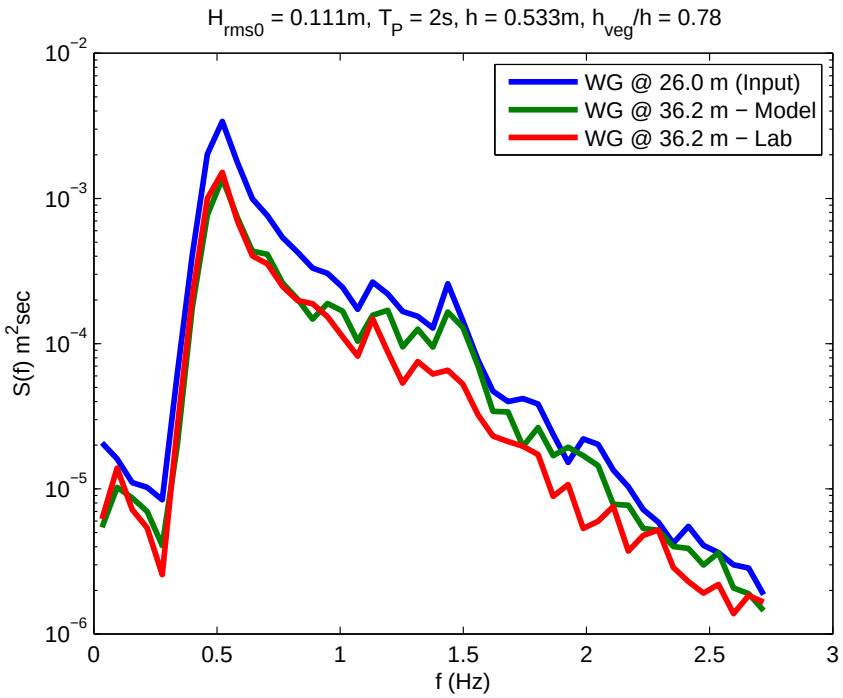

Fig 17: Spectral evolution comparison for Test 3

We can observe that, while the maximum damping is seen at peak frequency (f_{peak} = 0.67 and 0.5 Hz, respectively), the model tends to over predict the evolution of second harmonic peak (f_{peak} = 1.33 and 1 Hz, respectively) in both the cases. The error in prediction of spectral tail by the model is quantified in the following table using spectral energy predicted by the model and lab data available at Gauge 10, located at 9.3 m from beginning of vegetation. The root-mean-square value of difference between model and lab data is expressed in percentage of spectral energy in the peak frequency.

Table 3: Error in prediction of spectral evolution by model at Gauge 10

	f_P (Hz)	H_{RMS} (m)	h_{veg}/h	RMS error in spectral tail as % of peak spectral energy	Total RMS error as % of peak spectral energy
Test 1	0.667	0.111	0.78	2.08	2.34
Test 3	0.500	0.111	0.78	2.28	3.38
Test 6	0.667	0.081	0.91	5.17	5.67
Test 12	0.500	0.192	0.91	1.05	8.95

In Tests 1 and 3, we can see that the error in spectral tail evolution constitutes a large part of total error. This could be due to inadequacy of the mechanism employed to distribute the dissipation effect over the spectrum, which may not have resulted in the appropriate amounts of energy exchange between the harmonics. Also, in the laboratory conditions, development of standing wave, would have suppressed the transfer of spectral energy from lower to higher harmonics, thereby limiting the evolution of second harmonic peak.

It is also to be noted that % error in Test 12, which has nearly twice the incident wave height than other tests, is significantly larger. This is an indication of lesser damping generated by the model due to use of velocity at stem head. In this case, as the incident wave energy is higher, the velocity profile will penetrate deeper into the water column. Thus, usage of velocity at stem head is inadequate in conditions where vegetation is near emergent and encounters higher wave energy, because even the lower

parts of stem will "feel" the propagation of waves over it. This also affects the nature of vegetation motion, which further contributes to its dissipation effects.

The exchange of spectral energy between various harmonics can also be studied using a metric called bi-coherence (Kim and Powers 1979) of interacting triads, in which three frequencies (f_k , f_m and f_{k+m}) are in "resonance" with each other. Bi-coherence is defined as $B(f_k, f_m) = \left\langle A_k A_m A_{k+m}^* \right\rangle$, where f_k and f_m are interacting frequencies and A represents the complex spectral amplitude of corresponding frequency. Bi-coherence correlates gains and losses of energy in any given frequency pair (f_k and f_m) with gains and losses of energy in a third resonant frequency (f_{k+m}).

We will adopt some useful terminology to help distinguish between different interactions. Interactions between triads (f_{peak} , f_{peak} and $2f_{peak}$) and (f_{peak} , $2f_{peak}$ and $3f_{peak}$) are termed "harmonic interactions" since they include the peak frequency and its harmonics, and ($0.5f_{peak}$, f_{peak} and $1.5f_{peak}$) is termed "off-harmonic interaction" and represent trading of energy to and from sub-harmonic frequencies.

Figures 18 and 20 show the bi-coherence of aforementioned triads for model runs of Tests 1 and 3 respectively. Figures 19 and 21 are the same metric as obtained from lab data.

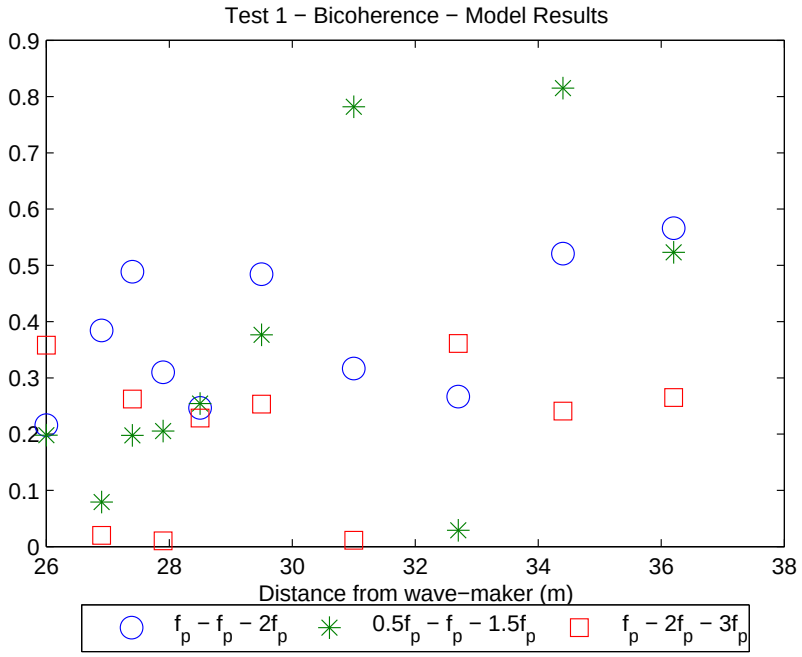

Fig 18: Bi-coherence plot for Test 1 using Model Results

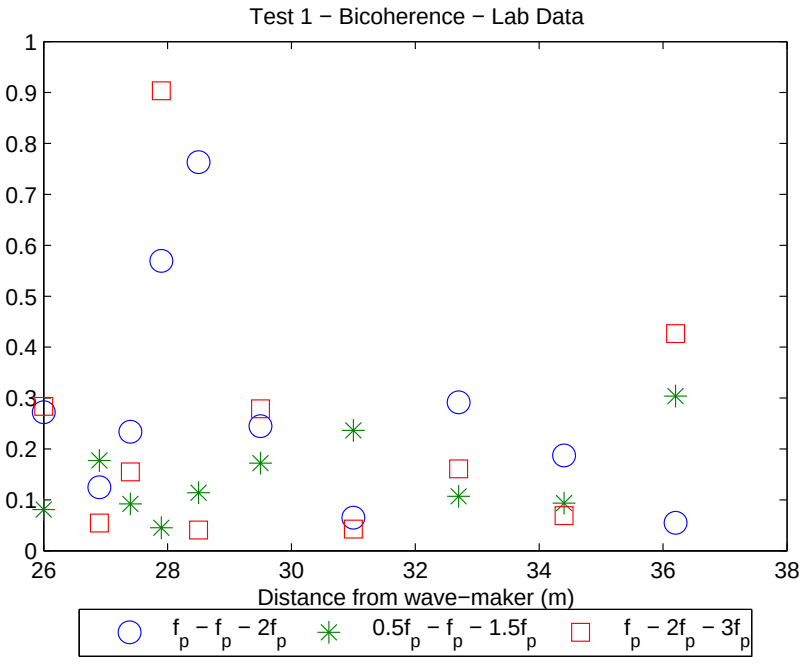

Fig 19: Bi-coherence plot for Test 1 using Lab Data

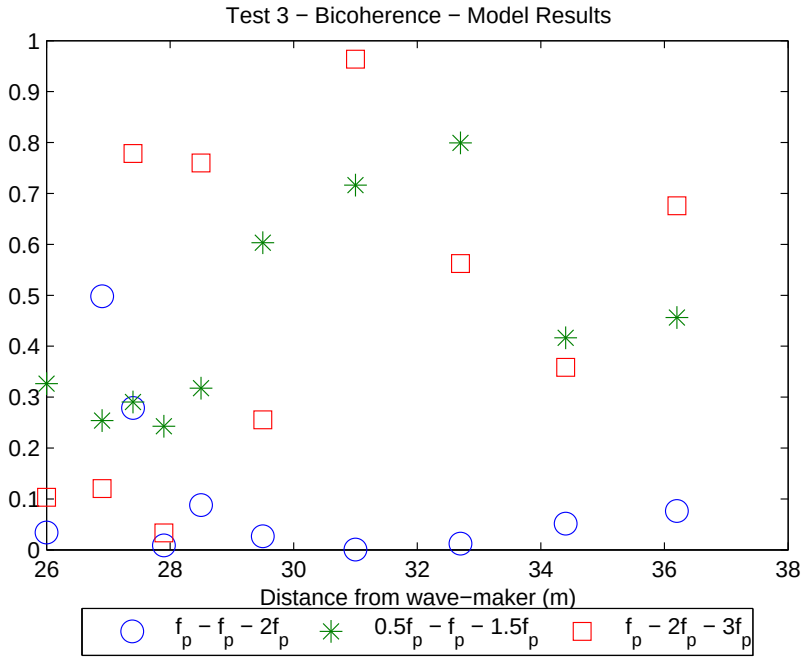

Fig 20: Bi-coherence plot for Test 3 using Model Results

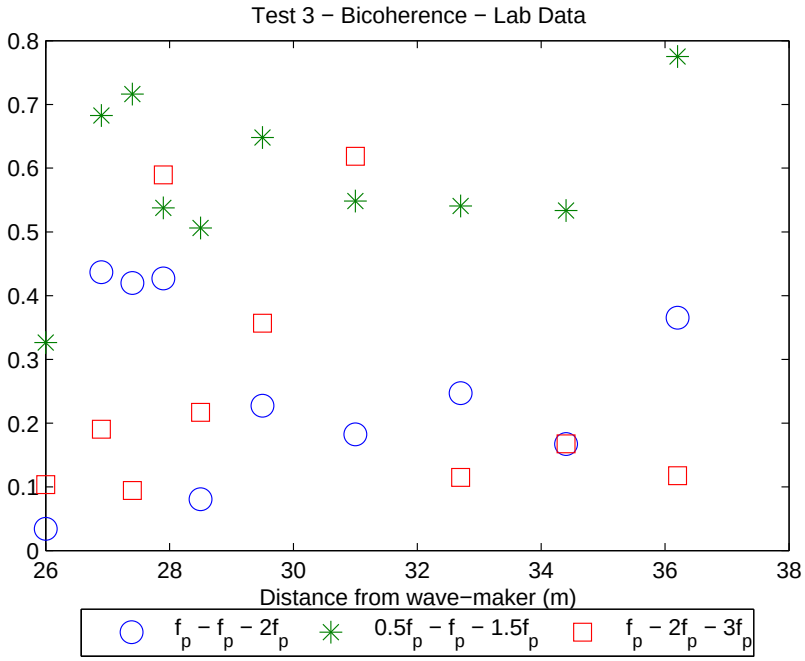

Fig 21: Bi-coherence plot for Test 1 using Lab Data

We can observe that the model tends to excite the off-harmonic transfer (denoted by the green star) of energy much more than that of in the Test 1 experiments, where it tends to be suppressed (Figs 18 and 19). This corroborates our earlier observation of development of second harmonic peak, which is non-existent in the laboratory conditions. While the same interaction is stronger in Test 3 (Fig 20), which is observed in the form of second harmonic peak in Fig 17, the model seems to transfer a little more energy than is seen in the experiment.

The red squares and blue circles, which represent the harmonic interactions of peak frequency, tend to be suppressed in Test 1 (Fig 19), which results in pronounced under evolution of spectral tail in laboratory conditions (Fig 16). As discussed earlier, this could be explained by possible presence of resonant standing waves, which could excite the flow of energy from peak to sub-harmonic frequencies (thereby suppressing harmonic interactions) and disrupt interaction with higher harmonics.

These observations are to be noted in contrast to the bi-coherence measurements of the same experiment (eg. Test 1) without the vegetation. As we can see in Fig 22, in wave propagation without vegetation, there is no marked suppression of any type of energy transfer. This means that the vegetation has a selective influence on the energy transfer between harmonics.

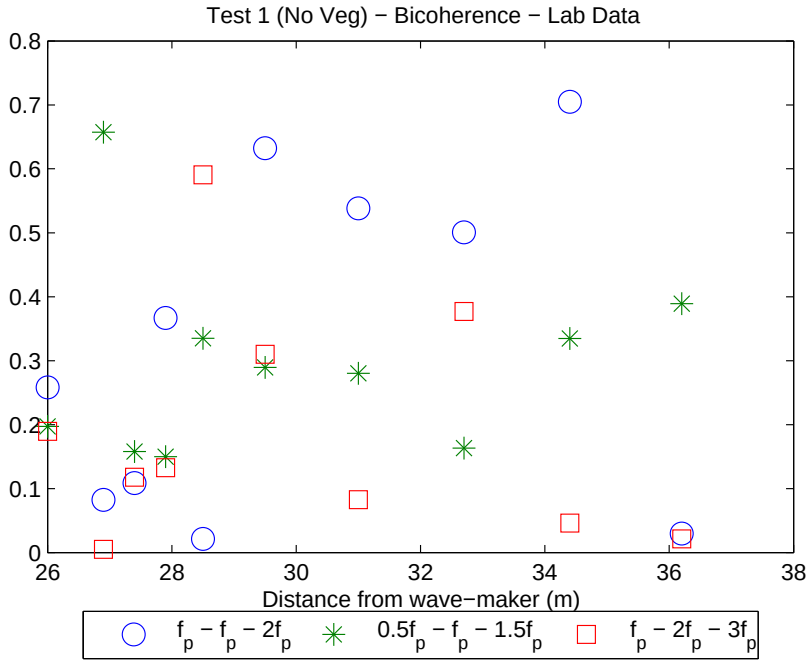

Fig 22: Bi-coherence plot of Test 1 from Lab Data: no vegetation

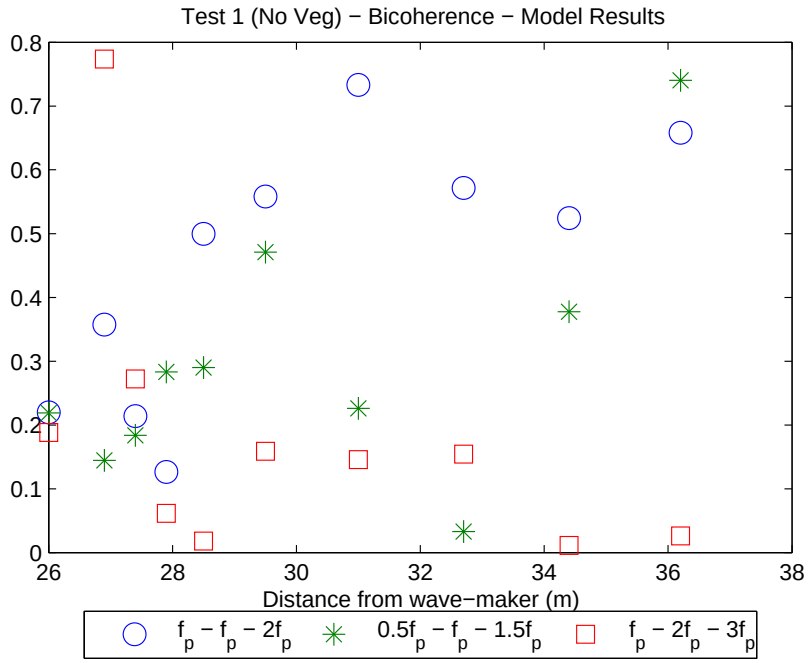

Fig 23: Bi-coherence plot of Test 1 from Model Result: no vegetation

The evolution of higher harmonics in a wave train can also be analyzed using study of evolution of a quantity called skewness. Skewness is defined as the asymmetry of wave shape with respect to horizontal axis. As the higher frequencies are excited in a wave train, the wave troughs flatten and crests sharpen, thereby resulting in a positive skewness of the wave shape. Skewness is defined as $\frac{\langle \eta^3 \rangle}{\langle \eta^2 \rangle^{3/2}}$.

Figures 24 and 25 show the evolution of skewness for Test 1 and 3 respectively.

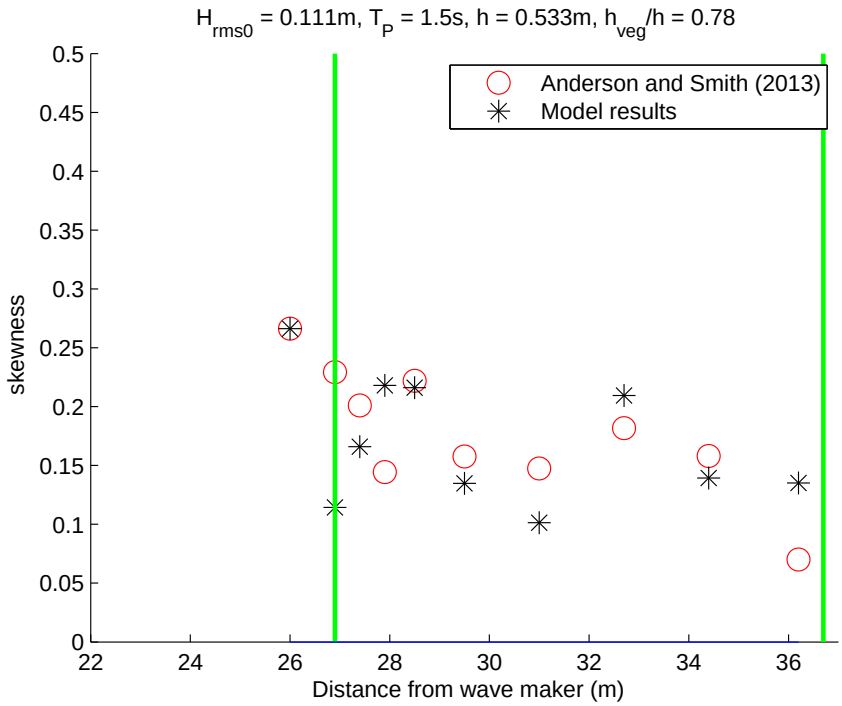

Fig 24: Evolution of wave shape skewness in Test 1

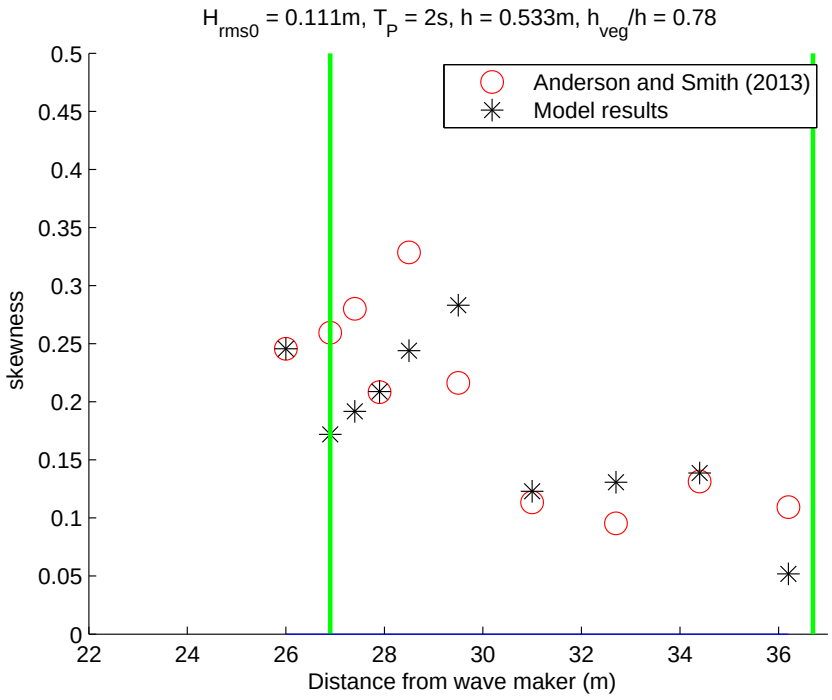

Fig 25: Evolution of wave shape skewness in Test 3

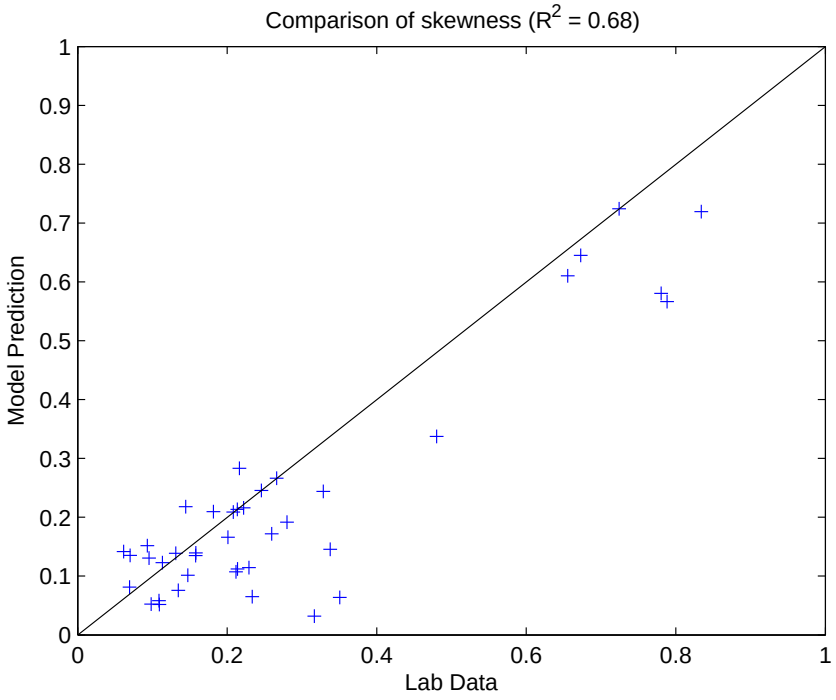

Fig 26: Model Prediction vs Lab Data Comparison for skewness

From the above figures, it can be observed that the model adequately simulates the general trend in both the cases (Fig 26: $R^2 = 0.68 > 0$). We can also note that in accordance with general observation all along, the transfer of energy to higher frequencies is suppressed, as the skewness tends to drop (although there is an initial increase) as the wave progress through the vegetation. But it is to be noted that more data is needed as skewness measurement improves when computed with more realizations.

CHAPTER V

CONCLUSIONS AND FUTURE WORK

5.1 Conclusions

The simulation of various laboratory experiments of waves over vegetation using the non-linear model described in this thesis has shown that damping due to vegetation is most accurately represented by using the formulation that accounts for sway motion of vegetation (Mendez et al. 1999a). It is also observed that the dissipation is most pronounced at the peak frequency and seems to affect other frequencies quite uniformly. But this could also be due to a destructive interference of variable energy exchange and skewed distribution of damping over frequencies. Further laboratory tests and more realizations (i.e., longer time series) are required to conduct sound analysis of bi-coherence interaction to determine the frequency dependency of damping behavior.

Harmonic energy transfer to higher frequencies is apparently effectively damped out due to presence of vegetation. This is due to the fact that second harmonic peak is very weakly evolved in the cases observed so far. The sub-harmonic energy exchange, which corresponds to long wave generation, is also damped, but not to the same extent as the peak-peak-2*peak interactions. But further studies need to be conducted to determine the existence or generation of standing waves, which could excite the sub-harmonic energy in the spectra. Experiments with longer duration, would help in discretizing the spectrum more finely, thereby leading to a closer inspection of sub-harmonic energy evolution.

The model performs very well in tracking the evolution of bulk characteristic such as H_{RMS}, thus validating this damping mechanism and subsequently, this formulation could be integrated with phase-averaged nearshore circulation models. This model also adequately simulates spectral and skewness evolution, although, it tends to over predict spectral tail evolution (Table 3).

5.2 Future Work

The scope of future work remains focused on correlating the drag coefficient to the energy dissipation due to presence of plant stems, using means which are listed below:

1. Throughout the simulation, model uses velocity at stem head to compute the Reynolds number and correspondingly, the drag coefficient. But this method may lead to inadequate representation of damping due to vegetation, if either the vegetation is more than 80% of water column (as in the case of Test 6) or if the root-mean-square wave height is substantially greater than the current values (Test 12). In the latter case, the velocity profile will be much more pronounced as we go deeper. Therefore, we propose usage of depth averaged velocity to determine the drag coefficient, which will be a definitive improvement over the current methodology.
2. One more avenue of improvement could be to rework the model using a different depth dependency in the boundary value problem, as opposed to the hyperbolic cosine in the existing wave theory, which accounts for the

presence of vegetation. In this case it is possible that, there would be a distinct depth dependency for each of the different categories of wetlands.

3. Analyze the lab data to filter any infra-gravity or standing waves in the vegetation region and rerun the model with filtered data to obtain a more consistent output from the model to that of corrected lab data.
4. Also, this model, which is based on evolution of spectrum, would better perform, if a probabilistic form of vegetation damping, akin to the one developed by Thornton and Guza (1983) for dissipation due to wave-breaking, is used.

REFERENCES

Allard, R., Dykes, J., Y.L. Hsu, Kaihatu, J. and Conley,D. (2008). "A real-time nearshore wave and current prediction system." *Journal of Marine Systems*, Volume 69, Issues 1–2, pp. 37-58, ISSN 0924-7963.

Anderson, M.E. and Smith, J.M. (2013). "Wave attenuation by flexible, idealized salt marsh vegetation." *Coastal Engineering,* Volume 83 (2014), pp. 82-92.

Asano T., Deguchi, H. and Kobayashi, N. (1992). "Interactions between water waves and vegetation." Proc. 23rd International Conf. on Coastal Engrg. in Venice, Italy, American Society of Civil Engineers, pp. 2710-2723.

Asano T., Tsutsui, S. and Sakai, T. (1988). "Wave damping characteristics due to seaweed." Proc. 35th Coast. Engrg. Conf. in Japan, Japan Society of Civil Engineers (JSCE), pp. 138-142.

Augustin, L.N., Irish, J.L. and Lynett, P. (2008). "Laboratory and numerical studies of wave damping by emergent and near-emergent wetland vegetation." *Coastal Engineering*, Volume 56 (2008), pp. 332-340.

Bailard, J.A. (1981). "An energetics total load sediment transport model for a plane sloping beach." *Journal of Geophysical Research*, Volume 86, No. C11, pp. 10,938-954.

Boczar-Karakiewicz, B. (1972). "Transformation of wave profile in shallow water – Fourier analysis." *Arch. Hydrotech.*, Volume 19, 197–209.

Bokaian, A. and Geoola, F. (1984). "Wake induced galloping of two interfering circular cylinders." *Journal of Fluid Mechanics*, Volume 146, pp. 383-415.

Booij, N., Ris, R.C. and Holthuijsen, L.H. (1999). "A third-generation wave model for coastal regions." *Journal of Geophysical Research*, Volume 104, No. C4, pp. 7649-66.

Bradley, K. and Houser, C. (2009). "Relative velocity of seagrass blades: Implications for wave attenuation in low-energy environments." *Journal of Geophysical Research*, Volume 114, F01004.

Bretschneider, C.L. (1952). "Revised wave forecasting relationships." *Proceedings of Second Conference on Coastal Engineering,* Council on Wave Research, 1952, pp. 1-5.

Bryant, P.J. (1973). "Periodic waves in shallow water." *Journal of Fluid Mechanics*, Volume 59, part 4, pp. 625-644.

Camfield, F.E. (1977). “Wind-wave propagation over flooded, vegetated land”. Tech. Paper No. 77-12, Coast. Engrg. Res. Ctr., U.S. Army Engineer Waterways Experiment Station, Vicksburg, Miss.

Chen, S-N., Sanford, L.P., Koch, E.W., Shi, F. and North, E.W. (2007). “A nearshore model to investigate the effects of seagrass bed geometry on wave attenuation and suspended sediment transport.” *Estuaries and Coasts*, Volume 30, No. 2, pp. 296-310.

Costanza, R., Perez-Maqueo, O., Martinez, M.L., Sutton, P., Anderson, S.J. and Mulder, K. (2008). “The value of coastal wetlands for hurricane protection.” *Ambio* 37, pp. 241–248.

Darlymple R.A., Kirby, J.T. and Hwang, P.A. (1984). “Wave diffraction due to areas of energy dissipation.” *Journal of Waterway, Port, Coastal and Ocean Eng.*, ASCE, Volume 110(1), pp. 67-79.

Dean, R.G. and Bender, C.J. (2006). “Static wave setup with emphasis on damping effects by vegetation and bottom friction.” *Coastal Engineering*, Volume 53 (2006), pp. 149-156.

Dean, R.G. and Dalrymple, R.A. (1984), “Water wave mechanics for Engineers and Scientists.” World Scientific Publishing , Hackensack, New Jersey.

Dubi, A. and Torum, A. (1994). “Wave damping by kelp vegetation.” In: Edge, B.L. (Ed.), *Proceedings of the Twenty-Fourth Coastal Engineering Conference.* ASCE, New York, pp.142-156.

Elgar, S. and Guza, R. (1985a). “Shoaling gravity waves: comparisons between field observations, linear theory and a nonlinear model.” *Journal of Fluid Mechanics*, Volume 158, pp. 44–70.

Elgar, S. and Guza, R. (1985b). “Observations of bispectra of shoaling surface gravity waves.” *Journal of Fluid Mechanics*, Volume 161, pp. 425-448.

Elgar, S. and Guza, R. (1988). “Nonlinear model predictions of bispectra of shoaling surface gravity waves.” *Journal of Fluid Mechanics,* Volume 167, pp. 1-18.

Foncesca, M.S. and Cahalan, J.A. (1992). “A preliminary evaluation of wave attenuation by four species of seagrass.” *Estuarine, Coastal and Shelf Science*, Volume 35, pp. 565-576.

Freilich, M.H. and Guza, R.T. (1984). “Nonlinear effects on shoaling surface gravity waves.” *Philosophical Translations of Royal Society of London*, Ser. A 311, 1–41.

Hammer, D.E. and Kadlec, R.H. (1986). “A model for wetland surface water dynamics.” *Water Resources Research*, Volume 22, No. 13, pp. 1951-58.

Kadlec, R.H. (1995). “Overview: Surface flow in constructed wetlands.” *Water Science and Technology*, Volume 32, No. 3, pp. 1-12.

Kaihatu, J.M. (2001). “Improvement of parabolic nonlinear dispersive wave model.” *Journal of Waterway, Port, Coastal and Ocean Eng.*, Volume 127, pp. 113-121.

Kaihatu, J.M. (2003). “Frequency domain wave models in the nearshore and surf zones,” in Lakhan, V.C. (ed.) *Advances in Coastal Modeling*, Elsevier, pp. 43-72.

Kaihatu, J.M. and Kirby, J.T. (1995). “Nonlinear transformation of waves in finite water depth.” *Physics of Fluids*, Volume 7(8), pp. 1903-1914.

Kaihatu, J.M. and Kirby, J.T. (1996). "Effects of mode truncation and dissipation in predictions of higher order statistics", *Proc. 25th Intl. Conf. Coast. Engrng.*, Orlando, pp. 123-136.

Kaihatu J.M., Sheremet, A. and Holland, K.T. (2007). “A model for the propagation of nonlinear surface waves over viscous muds”. *Coastal Engineering*, Volume 54(10), pp. 752-764.

Kiya, M., Tamura, H. and Arie, M. (1980). “Vortex shedding from a circular cylinder in moderate-Reynolds-number shear flow.” *Journal of Fluid Mechanics*, Volume 141, Part 4, pp. 721-735.

Knutson, P.L., Brochu, R.A., Seeling, W.N. and Inskeep, M. (1982). “Wave damping in *S.alterniflora* marshes.” *Wetlands*, Volume 2, pp. 87-104.

Kobayashi, N., Raichle, A.W. and Asano, T. (1993). “Wave attenuation by vegetation". *Journal of Waterway, Port, Coastal and Ocean Eng.*, Volume 119(1), 30-48.

Koehl, M.A.R (1986). “Seaweeds in moving water: form and mechanical function.” On the Economy of Plant Form and Function, edited by Givnish, T.J.

Leonard, L.A. and Luther, M.E. (1995). “Flow hydrodynamics in tidal canopies.” *Limnology Oceanography*, Volume 40(8), pp. 1474-84.

Liu, C. and Shen, Y-M. (2008). “Flow structure and sediment transport with impacts of aquatic vegetation”. *Journal of Hydrodynamics*, Ser. B, Volume 20(4), pp. 461-468.

Liu, P.L-F., Yoon, S.B. and Kirby, J.T. (1985). “Nonlinear refraction-diffraction of waves in shallow water.” *Journal of Fluid Mechanics*, Volume 153 (Apr), pp. 184-201.

Luo, S.C., Gan, T.L. and Chew, Y.T. (1996). "Uniform flow past one (or two in tandem) finite length circular cylinder(s)." *Journal of Wind Engineering and Industrial Aerodynamics*, Volume 59, pp. 6-93.

Macdonald, K. and Witek, B. (1994). "Management options for unstable bluffs in Puget Sound, Washington." Coastal Erosion Management Studies, Volume 8, Report 94-81.

Mase, H. and Kirby, J.T. (1992). "Hybrid frequency-domain KdV equation for random wave transformation." *Proceedings of the 23rd International Conference on Coastal Engineering*, Venice, Italy, pp. 474-487.

Mei, C.C. and Ünlüata, Ü. (1972). "Harmonic generation in shallow water waves." In:Meyer, R.E. (Ed.), *Waves on Beaches*. Academic Press, San Diego, CA, pp. 81–202.

Mendez, F.J and Losada, I.J. (2004). "An empirical model to estimate the propagation of random breaking and non-breaking waves over vegetation fields". *Coastal Engineering*, Volume 51(2004), pp. 103-118.

Mendez, F.J., Losada, I.J. and Losada, M.A. (1999a). "Hydrodynamics induced by wind waves in a vegetation field". *Journal of Geophysical Research*, Volume 104(C8), pp. 18383-18396.

Moeller, I., Spencer, T., French, J.R., Leggett, D.J. and Dixon, M. (1999). "Wave transformation over salt marshes: A field and numerical modelling study from North Norfolk, England, Estuarine." *Coastal and Shelf Science*, Volume 49, pp. 411-426.

Mottet, M. G. (1981). "Enhancement of the marine environment for fisheries and aquaculture in Japan." Department of Fisheries. State of Washington.

Nepf, H.M. (1999). "Drag, turbulence, and diffusion in flow through emergent vegetation." *Water Resources Research*, Volume 35, No. 2, pp. 479-489.

Nepf, H.M., Sullivan, J.A. and Zavistoski, R.A. (1997). "A model for diffusion within emergent vegetation." *Limnology Oceanography*, Volume 42(8), pp. 1735-45.

Peregrine, D.H. (1976). "Interaction of water waves and currents." *Advanced Applied Mechanics,* Volume 16, 9–117.

Philips, J.D. (1989). "Fluvial sediment storage in wetlands." *Water Resources Bulletin*, Volume 25, No. 4, pp. 867-873.

Phillips, O. M. (1960). "On the dynamics of unsteady gravity waves of finite amplitude. Part I. The elementary interactions." *Journal of Fluid Mechanics*, Volume 9, pp. 193-217.

Phillips, O. M. (1981a). “Wave interactions - the evolution of an idea.” *Journal of Fluid Mechanics*. Volume 106, pp. 215-27.

Powers, E.J. and Kim, Y.C. (1979). “Digital bispectral analysis and its applications to nonlinear wave interactions.” *IEEE Transactions on Plasma Science*, Volume PS-7, No. 2, pp. 120-131.

Price, W.A., Tomlinson, K.W. and Hunt, J.N. (1968). “The effect of artificial seaweed in promoting the build-up of beaches.” Coastal Engineering Proceedings, Volume 1(11).

Rogers, S.M. (1987). “Artificial seaweed for erosion control.” *Shore and Beach*, Volume 5(1), pp. 19-29.

Rogers, W., Kaihatu, J., Hsu, L., Jensen, R., Dykes, J., Holland, K. (2007). “Forecasting and hindcasting waves in the SWAN model in the Southern California Bight.” *Coastal Engineering*, Volume 54, pp. 1-15.

Sheremet, A. and Stone, G.W. (2003). “Observations of nearshore wave dissipation over muddy sea beds.” *Journal of Geophysical Research*, Volume 108, No. C11, pp. 3357.

Smith, R. and Sprinks, T. (1975). “Scattering of surface waves by conical island.” *Journal of Fluid Mechanics*, Volume 72, Part 2, pp. 373-384.

Thornton, E.B. and Guza, R.T. (1983). “Transformation of wave height distribution.” *Journal of Geophysical Research*, Volume 88, No. C10, pp. 5925-5938.

Tschirky, P., Hall, K. and Turcke, D. (2000). “Wave attenuation by emergent wetland vegetation.” *Coastal Engineering* 2000, pp. 865-877.

Wallace, S. and Cox, R. (2001). “Effects of seagrass on nearshore current and wave dynamics.” *Coastal Engineering* 2000, pp. 878-890.

Whalin, R.W. (1971). “Wave refraction theory in a convergence zone.” Coastal Engineering Proceedings, Volume 1(12).

Williams, G.D. and Thom, R.M. (2001), Marine and estuarine shoreline modification issues.